The Astrophysical Journal Letters, 983:L27 (16pp), 2025 April 10 https://doi.org/10.3847/2041-8213/adc4da

Uniting the Observed Dynamical Dark Energy Preference with the Discrepancies in Ω_m and H_0 across Cosmological Probes

Xianzhe TZ Tang[1], Dillon Brout[1,2], Tanvi Karwal[3], Chihway Chang[3,4], Vivian Miranda[5], and Maria Vincenzi[6]
[1] Boston University, Department of Astronomy, 725 Commonwealth Ave., Boston, MA 02215, USA; tztang@bu.edu, dbrout@bu.edu
[2] Boston University, Department of Physics, 725 Commonwealth Ave., Boston, MA 02215, USA
[3] Kavli Institute for Cosmological Physics, University of Chicago, Chicago, IL 60637, USA
[4] Department of Astronomy and Astrophysics, University of Chicago, Chicago, IL 60637, USA
[5] C. N. Yang Institute for Theoretical Physics, Stony Brook University, Stony Brook, NY 11794, USA
[6] Department of Physics, Oxford University, Oxford, UK
Received 2025 February 28; revised 2025 March 24; accepted 2025 March 25; published 2025 April 9

Abstract

Recent results from Type Ia supernovae, baryon acoustic oscillations (BAOs), and the cosmic microwave background (CMB) indicate (1) potentially discrepant measurements of the matter density Ω_m and Hubble constant H_0 in the ΛCDM model when analyzed individually and (2) hint of dynamical dark energy in a w_0w_aCDM model when data are combined in a joint analysis. We examine whether underlying dynamical dark energy cosmologies favored by data would result in biases in Ω_m and H_0 for each probe when analyzed individually under ΛCDM. We generate mock data sets in w_0w_aCDM cosmologies, fit the individual probes under the ΛCDM model, and find that expected biases in Ω_m are ∼0.03. Notably, the Ω_m differences between probes are consistent with values observed in real data sets. We also observe that mock DESI-BAO data sets generated in the w_0w_a CDM cosmologies will lead to a biased measurement of H_0 higher by $\sim 1.2\ \mathrm{km\ s^{-1}\ Mpc^{-1}}$ when fitted under ΛCDM, appearing to mildly improve the Hubble tension, but as the true underlying H_0 is lower, the tension is in fact worsened. We find that the Ω_m discrepancies, the high BAO H_0 relative to the CMB, and the joint dynamical dark energy signal are all related effects that could be explained simultaneously with either new physics or new systematics. While it is possible to unite many of the discrepancies seen in recent analyses along a single axis, our results underscore the importance of understanding systematic differences in data sets, as they have unique impacts in different cosmological parameter spaces.

Unified Astronomy Thesaurus concepts: Cosmology (343); Cosmological parameters (339); Dark energy (351); Cosmological constant (334); Dynamical evolution (421); Cosmic microwave background radiation (322); Baryon acoustic oscillations (138); Type Ia supernovae (1728)

1. Introduction

The standard ΛCDM cosmological model, which includes a cosmological constant dark energy Λ and cold dark matter (CDM), has historically been remarkably successful in explaining a wide range of cosmological observations, from measurements of the cosmic microwave background (CMB; Planck Collaboration 2020) to Type Ia supernovae (SNe Ia; D. Brout et al. 2022a; DESI Collaboration 2024).

However, recent measurements of baryon acoustic oscillations (BAO) from the Dark Energy Spectroscopic Instrument (DESI) and SNe from the Dark Energy Survey (DES) have revealed intriguing discrepancies in the value of Ω_m under the ΛCDM model when compared to other analyses with CMB and SN data. Specifically, BAO data from DESI Y1 tend to favor lower values of $\Omega_m = 0.295 \pm 0.015$ (DESI Collaboration 2025), and the new DESI full-shape modeling of clustering measurements with big bang nucleosynthesis (BBN) and scalar spectral index priors finds $\Omega_m = 0.2962 \pm 0.0095$ (DESI Collaboration 2025). On the other hand, SN data sets prefer higher values. For instance, $\Omega_m = 0.353 \pm 0.017$ from DES-SN 5YR (DESI Collaboration 2024; M. Vincenzi et al. 2024; B. O. Sánchez et al. 2024), $\Omega_m = 0.331 \pm 0.018$ from PantheonPlus (D. Brout et al. 2022a; D. Scolnic et al. 2022), and $\Omega_m = 0.359 \pm 0.027$ from Union3 (D. Rubin et al. 2023). Although these differences do not reach the 3σ threshold for significant tension, they hint at possible inconsistencies among the data sets, with statistical deviations of 1.6σ for PantheonPlus, 2.0σ for Union3, and 2.6σ for DES-SN 5YR when compared to DESI results (DESI Collaboration 2025). Further quantifying this tension, K. V. Berghaus et al. (2024) analyzed the combined CMB+DESI+DES-SN 5YR data (CMB being Planck C_ℓ^{TTTEEE} restricted to $\ell < 1296$) and observed a $\Delta\chi^2$ of approximately 8.5 when $\Omega_m = 0.295$, corresponding to the best-fit value from DESI BAO measurements. This χ^2 difference translates to a tension of approximately 2.9σ, indicating a significant deviation in Ω_m between the SN data sets and the DESI BAO preferred cosmology.

In addition to discrepancies in Ω_m, recent observations have revealed differences in the Hubble constant (H_0) between BAO and CMB measurements. The DESI Y1 BAO results (DESI Collaboration 2025), when combined with calibrations of the sound horizon r_d from the CMB (Planck Collaboration 2020) or BBN (V. Mossa et al. 2020), yield higher H_0 values than the CMB itself. Specifically, DESI Y1 BAO find $H_0 = 69.29 \pm 0.87\ \mathrm{km\ s^{-1}\ Mpc^{-1}}$ with r_d from the CMB or $H_0 = 68.53 \pm 0.80\ \mathrm{km\ s^{-1}\ Mpc^{-1}}$ with a BBN prior (DESI Collaboration 2025). Recently, the DESI 2024 VII full shape with BBN and n_{s10} prior shows $H_0 = 68.56 \pm 0.75\ \mathrm{km\ s^{-1}\ Mpc^{-1}}$ (DESI Collaboration 2025). These BAO values are notably higher than the

$H_0 = 67.27 \pm 0.60$ km s^{-1} Mpc^{-1} (TT, TE, EE, LowE) reported by the Planck 2018 CMB analysis (Planck Collaboration 2020) by about 1–2 km s^{-1} Mpc^{-1}. While these differences in H_0 between BAO and CMB are not at the level of the Hubble tension between Planck and SH0ES-calibrated SNe ($\sim$6 km s^{-1} Mpc^{-1} at $>5\sigma$; A. G. Riess et al. 2022), it is a notable difference that has withstood several recent analyses.

Moreover, and perhaps most notably, recent analyses have also hinted at the possibility of evolving dark energy when all data sets (SN, BAO, CMB) are combined (D. Brout et al. 2022a; DESI Collaboration 2024; DESI Collaboration 2025). Specifically, the phenomenological Chevallier–Polarski–Linder (CPL) parameterization w_0w_aCDM is often employed[7] to explore evolving dark energy cosmologies, wherein the dark energy equation of state

$$w(a) = w_0 + w_a(1 - a), \tag{1}$$

where w_0 is the value of the equation of state today (or at $a = 1$) and w_a describes the rate of change of the equation of state with the scale factor a. Both w_0 and w_a are constants. Analyses using w_0w_aCDM show deviations from the ΛCDM framework at significant levels when combining the DESI BAO (DESI Collaboration 2025) with SNe: 2.5σ using Pantheon+ (D. Brout et al. 2022a), 3.5σ with Union3 (D. Rubin et al. 2023), and 3.9σ with DES (DESI Collaboration 2024). With DESI 2024 VII full-shape results, the combined probes' preference for $w_0 > -1$ and $w_a < 0$ is reinforced (DESI Collaboration 2025a). These observations align with findings from K. V. Berghaus et al. (2024), who explored scalar field models of dark energy using DESI BAO data in combination with CMB and SN measurements. They found that models allowing for a small but nonzero kinetic energy in scalar fields can reduce the tension in the matter density parameter Ω_m between BAO and SN data sets.

Motivated by DESI Y1 results (DESI Collaboration 2025), we aim to investigate the question whether a true w_0w_aCDM cosmology could naturally manifest the observed differences in Ω_m and H_0 when SN, BAO, and CMB data sets are analyzed separately under the ΛCDM framework, by generating mock w_0w_aCDM cosmological data. While it is expected that assuming an incorrect expansion history can lead to biases in the inferred values of cosmological parameters like Ω_m and H_0, the crucial question is whether the specific discrepancies observed in the real data sets are consistent with what would be expected if the true underlying cosmology deviates from ΛCDM and follows the w_0w_aCDM model preferred by combined data.

Ultimately, we aim to clarify whether the Ω_m tensions between SN, BAO, and CMB data sets signify new physics that may be explained by dynamical dark energy.

This Letter is organized as follows: In Section 2, we introduce our simulations of SNe, BAO, and CMB, respectively. In Section 3, we discuss our methodology and show results. Finally, in Section 4, we discuss the implications of this work. Throughout, we assume units of km s^{-1} Mpc^{-1} for H_0.

[7] It is important to note that while many studies use the simplistic w_0w_aCDM model that allows for dynamical deviations from a cosmological constant Λ, it is not necessarily a preferred model, and other evolving dark energy models are often examined (e.g., S. R. Brownsberger et al. 2019; S. Dhawan et al. 2020; J. Rebouças et al. 2025; R. Camilleri et al. 2025).

2. Simulations and Likelihood

To investigate the impact of cosmological model assumptions on parameter estimation, we generate mock data sets for SNe Ia, BAOs, and the CMB. For simplicity, we construct idealized mock data sets with realistic uncertainties, but without adding observational noise or scatter. This approach allows us to focus on the effects of cosmological models on the data without the complications introduced by statistical fluctuations or selection effects. Throughout this Letter we assume flatness.

2.1. Type Ia Supernovae

Mock Data: We simulate a data set of 1829 SNe Ia, using the same redshifts as the Dark Energy Survey Supernova Program Year 5 (DES-SN 5YR) sample (DESI Collaboration 2024). This data set covers a redshift range of $0.02 < z < 1.12$ and provides a DES Y5–like sample as the SN probe.

Simulation Method: The simulated SN Ia data are generated by computing the distance modulus $\mu(z)$ for each SN using the background cosmological model. The distances correspond exactly to the model without added scatter, ensuring that any deviations in parameter estimation arise solely from the model assumptions. The distance modulus (or luminosity distance $d_L(z)$) is calculated as

$$\mu(z) = m - M = 5\log_{10}\left(\frac{d_L(z)}{10\,\mathrm{pc}}\right), \tag{2}$$

where for the DES (uncalibrated) SNe the measured quantity is the apparent magnitude m and where the intrinsic absolute magnitude M of an SN is unknown.

Thus, M is a parameter that is fully degenerate with H_0, and thus both parameters (M, H_0) are marginalized over in the likelihood fit.

By following this methodology, our analysis closely imitates the DES-SN 5YR likelihood, as standard practices in SN cosmology incorporate these nuisance parameters.

Uncertainties: We adopt the measurement uncertainties on $\mu(z)$ for each SN and covariance $\boldsymbol{C}_{\mathbf{DES}}$ from the public DES-SN 5YR data set itself (DESI Collaboration 2024).

Likelihood: To account for uncertainties in the absolute magnitude M and the Hubble constant H_0, we introduce these as additional free parameters and marginalize over M in the likelihood function. Following the methodology outlined in DESI Collaboration (2024), the likelihood function for the SNe Ia is defined as

$$\ln \mathcal{L}_{\mathrm{SNe}} = -\frac{1}{2}[\boldsymbol{\Delta\mu}^T \cdot \mathbf{C}_{\mathrm{DES}}{}^{-1} \cdot \boldsymbol{\Delta\mu} + \ln((2\pi)^N|\boldsymbol{C}_{\mathrm{DES}}|)], \tag{3}$$

where $\Delta\mu$ represents the residual vectors between the model predictions and the observed (mock) data. This modified likelihood function allows us to analytically marginalize over the nuisance parameter M, effectively removing its dependence from the cosmological parameter estimation.

2.2. Baryon Acoustic Oscillations

Mock Data. The BAO data are simulated to match observations from DESI Y1 results (DESI Collaboration 2025). This includes measurements from seven different tracers across different effective redshifts, providing constraints on the expansion rate and geometry of the Universe.

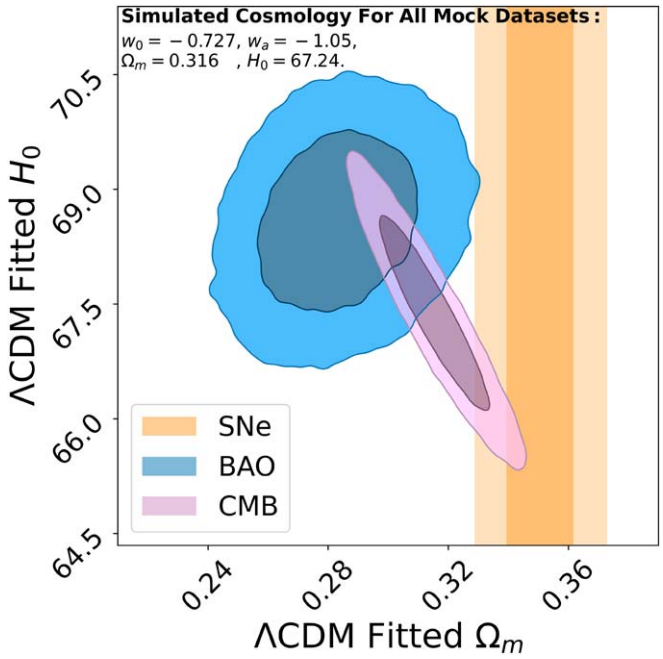

Figure 1. Constraints on Ω_m and H_0 obtained by fitting ΛCDM to mock CMB, BAO, and SN data sets generated in the DESI+DES-SN+Planck (DESI Collaboration 2025) best-fit w_0w_aCDM cosmology $\{w_0 = -0.727,\ w_a = -1.05,\ \Omega_m = 0.316,\ H_0 = 67.24\}$. The contours represent the 68% and 95% confidence regions for each mock data set individually: SNe (yellow), BAO (blue), and CMB (pink). This figure illustrates the Ω_m and H_0 discrepancies between different probes when fitting ΛCDM to data simulated in a dynamical w_0w_aCDM cosmology.

Simulation Method. From the background cosmology model, we compute the BAO observables: the angle-averaged distance $D_V(z)$, and the Alcock–Paczyński parameters $F_{\rm AP}(z)$, defined as ratio of transverse to line-of-sight comoving distances . The angle-averaged distance is

$$D_V(z) = [zD_M^2(z)D_H(z)]^{1/3}, \tag{4}$$

where $D_M(z)$ is the comoving angular diameter distance and $D_H(z) = c/H(z)$ is the Hubble distance. The comoving distances and Hubble parameters are calculated using `astropy.cosmology` (T. P. Robitaille et al. 2013). The ratio $F_{\rm AP}(z)$ of transverse to line-of-sight comoving distances is

$$F_{\rm AP}(z) = \frac{D_M(z)}{D_H(z)}. \tag{5}$$

We note that our method uses $D_V(z)/r_d$ and $F_{\rm AP}(z)$, while DESI Y1 uses D_M/r_d, D_H/r_d, and D_V/r_d, but they are equivalent. For the drag-epoch sound horizon r_d, we use[8] Equation (2.5) from the DESI Y1 cosmology paper DESI Collaboration (2025). We apply a Gaussian distribution from BBN on $\Omega_b h^2 = 0.02218 \pm 0.00055$ (V. Mossa et al. 2020) in the Markov Chain Monte Carlo (MCMC) analysis in Figure 1. However, for the Hessian matrix maximization analyses in this work (used in Section 3.2), for computational feasibility, we use the central value $\Omega_b h^2 = 0.02218$ from BBN constraints (V. Mossa et al. 2020). See each method in Section 3.1 for details.

Uncertainties: Uncertainties and correlations between D_V, D_M, and D_H are adopted from Table 1 of the DESI Y1 cosmology paper (DESI Collaboration 2025). For tracers where both D_M and D_H are provided, we calculate the uncertainties in D_V and $F_{\rm AP}$ using error propagation formulae, accounting for the correlation coefficient r between D_M and D_H. The uncertainty in D_V is

$$\sigma_{D_V} = \frac{D_V}{3}\sqrt{4\left(\frac{\sigma_{D_M}}{D_M}\right)^2 + \left(\frac{\sigma_{D_H}}{D_H}\right)^2 + 4r\frac{\sigma_{D_M}}{D_M}\frac{\sigma_{D_H}}{D_H}}. \tag{6}$$

Similarly, the uncertainty in $F_{\rm AP}$ is

$$\sigma_{F_{\rm AP}} = F_{\rm AP}\sqrt{\left(\frac{\sigma_{D_M}}{D_M}\right)^2 + \left(\frac{\sigma_{D_H}}{D_H}\right)^2 - 2r\frac{\sigma_{D_M}}{D_M}\frac{\sigma_{D_H}}{D_H}}, \tag{7}$$

where r represents the correlation between D_M and D_H given in Table 1 of DESI Collaboration (2025).

For the five of seven tracers from DESI where both D_M and D_H are available, we use both $D_V(z)/r_d$ and $F_{AP}(z)$. For the remaining two tracers with only D_V provided, we use just $D_V(z)/r_d$ as the basis of the data for simulations.

Likelihood: The likelihood function for BAO is defined as

$$\ln \mathcal{L}_{\rm BAO} = -\frac{1}{2}\left[\sum_i\left(\frac{M_i - T_i}{\sigma_i}\right)^2 + \sum_i \ln(2\pi\sigma_i^2)\right], \tag{8}$$

with observed (or mock) BAO data M_i for D_V/r_d and F_{AP}, theoretical predictions T_i from the cosmological model, and uncertainties σ_i from DESI Y1 papers (DESI Collaboration 2025).

Table 1
Uncertainties (Standard Deviations; Top) and Correlation Coefficients (Bottom) between the Shift Parameter R and the Acoustic Scale l_A from the Planck 2018 TT, TE, EE + lowE Analysis for the ΛCDM Cosmological Model (Planck Collaboration 2020)

	Parameter Uncertainty σ
R	0.0065
l_A	0.105
	Correlation Coefficients
	R l_A
R	1.0 0.47
l_A	0.47 1.0

2.3. Cosmic Microwave Background

Mock Data: We incorporate constraints from CMB using two parameters—the acoustic scale l_A and the shift parameter R. The uncertainties on these parameters and the physical baryon density used in our calculations are derived from the Planck 2018 results and covariance (Planck Collaboration 2020).

Simulation Method: The shift parameter R and the acoustic scale l_A are calculated as (E. Komatsu et al. 2009)

$$R = \sqrt{\Omega_m H_0^2}\frac{D_M(z_*)}{c},$$

$$l_A = (1 + z_*)\frac{\pi D_M(z_*)}{r_s(z_*)},$$

where $D_M(z_*)$ is the comoving angular diameter distance to the photon-decoupling redshift z_*, $r_s(z_*)$ is the comoving sound

[8] We have also incorporated a direct calibration of r_d; please see Appendix C.

Table 2
Comparison of the ΛCDM Fits to Real and Mock Data, and the *p*-values Assessing the Agreement of Ω_m among Different Probes, as Described in Equation (13)

Data/Mock	ΛCDM Fit	Ω_m Agreement between Probes (See Section 3.1)
Real data (DESI Y1 VI BAO, DES-SN 5YR, Planck18 CMB)	BAO: $\Omega_m = 0.295 \pm 0.015$, $H_0 = 68.5 \pm 0.8$ SNe: $\Omega_m = 0.353 \pm 0.017$ CMB: $\Omega_m = 0.315 \pm 0.007$, $H_0 = 67.3 \pm 0.6$	p-value = 0.035
Mock simulated in DESI+CMB best-fit ΛCDM$\Omega_m = 0.31$, $H_0 = 68$	BAO: $\Omega_m = 0.311 \pm 0.019$, $H_0 = 68.0 \pm 0.8$ SNe: $\Omega_m = 0.310 \pm 0.011$ CMB: $\Omega_m = 0.310 \pm 0.012$, $H_0 = 68.0 \pm 0.8$	p-value = 0.999
Mock simulated in DESI+CMB+DESY5SN best-fit w_0w_aCDM$\Omega_m = 0.316$, $w_0 = -0.727$, $w_a = -1.05$, $H_0 = 67.24$	BAO: $\Omega_m = 0.281^{+0.019}_{-0.016}$, $H_0 = 68.6 \pm 0.8$ SNe: $\Omega_m = 0.350 \pm 0.011$ CMB: $\Omega_m = 0.315 \pm 0.012$, $H_0 = 67.4 \pm 0.8$	p-value = 0.003
Mocks simulated for each step in DES24 (DES-SNY5 + eBOSS + Planck18 + 3x2pt) w_0w_aCDM chain	BAO: $\Omega_m = 0.303^{+0.051}_{-0.043}$, $H_0 = 67.8^{+1.3}_{-1.8}$ SNe: $\Omega_m = 0.355^{+0.055}_{-0.049}$ CMB: $\Omega_m = 0.321^{+0.030}_{-0.023}$, $H_0 = 66.9^{+1.5}_{-2.3}$	68% of p-values within $[9 \times 10^{-6}, 0.17]$

Note. A smaller p-value indicates more discrepancies on Ω_m among probes. Each row corresponds to a different data/mock scenario. Row 1: results from fits to real observational data (DESI Collaboration 2025; DESI Collaboration 2024; Planck Collaboration 2020), providing a baseline for comparison with mock scenarios. Row 2: a null test with mocks simulated under a common ΛCDM cosmology, showing a p-value close to 1, indicating agreement between fitted Ω_m. Row 3: same as described in Section 3.1 and illustrated in Figures 1 and 2. Row 4: the 68% credible interval of best-fit parameters for fits to the DES24 chain cosmologies, which is also described in Section 3.2 and illustrated in Figure 3.

horizon at z_*, and c is the speed of light. Note that r_{z_*} is physically different from the drag-epoch sound horizon r_d in the BAO section.

The redshift of photon decoupling, z_*, is calculated using the fitting formula from Equation (8) of L. Chen et al. (2019), which takes the physical baryon density $\Omega_b h^2$ and Ω_m as input and can be adjusted to the chosen cosmology. As done for BAO mocks (Section 2.2), for computational feasibility, we take the BBN constraint of $\Omega_b h^2 = 0.02218$ (V. Mossa et al. 2020) for our Hessian matrix maximization analyses in Section 3.2, whereas for the MCMC analysis done in Figure 1 we use a Gaussian BBN prior on $\Omega_b h^2 = 0.02218 \pm 0.00055$ (V. Mossa et al. 2020).

The comoving angular diameter distance and the comoving sound horizon $r_s(z_*)$ at z_* are computed using numerical integration routines from `SciPy` (P. Virtanen et al. 2020) and `Astropy` (T. P. Robitaille et al. 2013) with Equation (3) from L. Chen et al. (2019).

Uncertainties: We adopt the uncertainties and covariance between R and l_A from the Planck 2018 results (Planck Collaboration 2020). The covariance matrix is given by

$$\boldsymbol{C_{P18}} = \begin{pmatrix} \sigma_R^2 & \sigma_{Rl_A} \\ \sigma_{Rl_A} & \sigma_{l_A}^2 \end{pmatrix}, \tag{9}$$

with the variances and covariance specified from the Planck 2018 TT, TE, EE+lowE likelihoods shown in Table 1.

Since we are generating idealized simulated data, the observed values $R_{\rm obs}$ and $l_{A,\rm obs}$ correspond exactly to the theoretical values computed from the underlying cosmological model without added noise.

Likelihood: The likelihood function for the CMB is computed by comparing the theoretical values of R and l_A with the observed values, incorporating the covariance between these parameters. The negative log-likelihood is given by

$$\ln \mathcal{L}_{\rm CMB} = -\frac{1}{2}[\Delta \boldsymbol{d}^{\rm T} \cdot \boldsymbol{C}_{\boldsymbol{P18}}^{-1} \cdot \Delta \boldsymbol{d} + \ln(2\pi |\boldsymbol{C_{P18}}|)], \tag{10}$$

where $\Delta \boldsymbol{d}$ is the difference vector

$$\Delta \boldsymbol{d} = \begin{pmatrix} R_{\rm theory} - R_{\rm obs} \\ l_{A,\rm theory} - l_{A,\rm obs} \end{pmatrix}. \tag{11}$$

3. Analysis

In this section, we explore how discrepancies in Ω_m and H_0 between different cosmological probes might manifest if the true underlying cosmology is w_0w_aCDM but it is analyzed within the ΛCDM framework. Our analysis consists of two main parts. First, we examine the single dynamical dark energy cosmology derived in DESI Collaboration (2025) from the best-fit results of the combined DESI+DES+Planck data.

Second, to evaluate the probabilities of occurrences of differences in Ω_m and H_0 across the different probes, we sample from the entire observed posterior distribution of the w_0w_aCDM model. We then compare these differences among the different probes with the discrepancy found in the real data sets.

3.1. Single Realization from a Best-fit w_0w_aCDM

In this section, we first calculate the probability of obtaining the observed constraints in ΛCDM for each probe individually if the true underlying cosmology is w_0w_aCDM. First, we create mock data sets {SNe, BAO, CMB} in the DESI+DES+Planck w_0w_aCDM best-fit cosmology $\{w_0 = -0.727, w_a = -1.05, \Omega_m = 0.316, H_0 = 67.24\}$. We then fit each mock data set individually in ΛCDM with an MCMC, applying a Gaussian distribution on the physical baryon density $\Omega_b h^2 = 0.02218 \pm 0.00055$ from BBN (V. Mossa et al. 2020) for the BAO and CMB fits. We float Ω_m and H_0 as free parameters, while $\Omega_b h^2$ is constrained by the prior. As shown in Figure 1 and Table 2, we find that the best-fit values of Ω_m under ΛCDM for each data set are $\Omega_{m,\rm SNe} = 0.35 \pm 0.012$, $7{\rm D}1\Omega_{m,\rm BAO} = 0.28 \pm 0.018$, and $7{\rm D}1\Omega_{m,\rm CMB} = 0.315 \pm 0.012$. These values are consistent with those observed in the real data sets, as reported by DES-SN 5YR SNe ($\Omega_m = 0.353 \pm 0.017$; DESI Collaboration 2024),

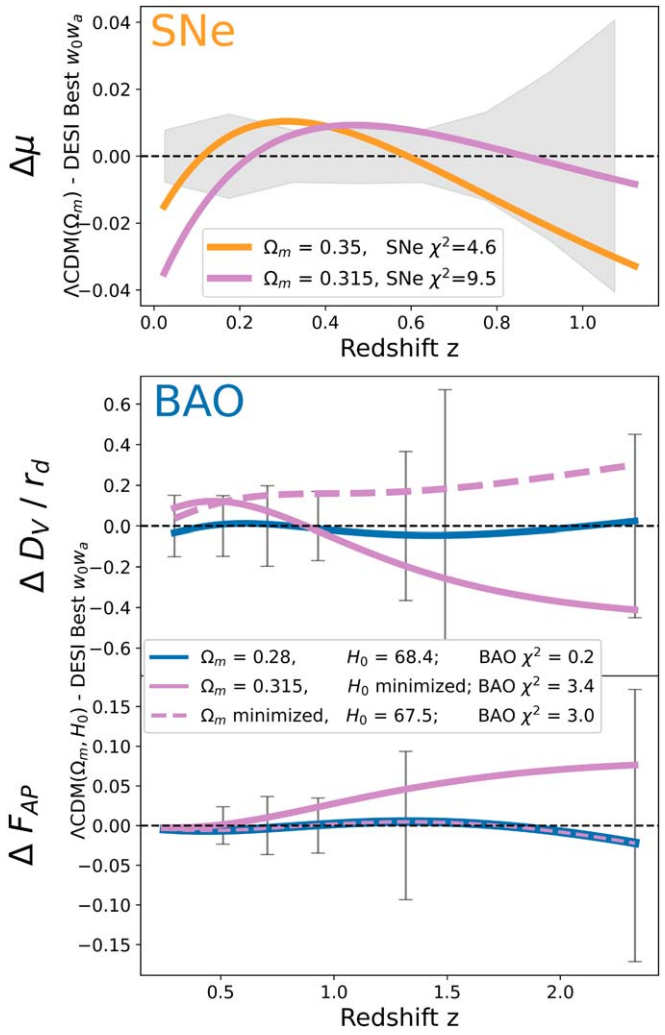

Figure 2. Comparison between the best-fit ΛCDM cosmology (with $\Omega_m = 0.35$ for SNe or $\Omega_m = 0.28$ for BAO) and a Planck-like ΛCDM cosmology ($\Omega_m = 0.315$) against the DESI+CMB+DESY5SN (DESI Collaboration 2025) best-fit w_0w_aCDM model $\{w_0 = -0.727,\ w_a = -1.05,\ \Omega_m = 0.316,\ H_0 = 67.24\}$ with realistic data uncertainties shown for SNe (top) and BAO (bottom). The three panels show residuals in the SN distance modulus μ, the BAO D_V/r_d, and the BAO F_{AP} vs. redshift z. Error bars (shaded regions) reflect uncertainties in DES-SN 5YR (DESI Collaboration 2024) and DESI Y1 (DESI Collaboration 2025), with binned SN errors using weighted averages of uncertainties in redshift bins of width $\Delta z = 0.15$ for illustration. The χ^2 values reported indicate goodness of fit for each model (colored curves) relative to the mock data generated in w_0w_aCDM (horizontal dashed), calculated similarly to Equations (3) and (8) (without the normalization term). "Minimized" refers to floating one parameter while fixing others to achieve the lowest χ^2. For BAO, when $\Omega_m = 0.315$, H_0 is "minimized" to 68.8; when $H_0 = 67.5$, Ω_m is "minimized" to 0.279. For the SNe, H_0 is also "minimized" for both models presented.

DESI BAO ($\Omega_m = 0.295 \pm 0.015$; DESI Collaboration 2025), and Planck 2018 CMB ($\Omega_m = 0.3166 \pm 0.0084$; Planck Collaboration 2020).

In order to illustrate why dynamical dark energy results in higher Ω_m for SNe and lower Ω_m for BAO, we show data vector residuals relative to the DESI (DESI Collaboration 2025) maximum likelihood w_0w_aCDM cosmology in Figure 2. For each probe (top: SNe; bottom: BAO), we show data vectors corresponding to both the best-fit ΛCDM cosmological parameters and Planck-like ΛCDM cosmological parameters (i.e., $\Omega_m = 0.315$). SN data favor a higher Ω_m to match the observed (uncalibrated) luminosity distances, while BAO data prefer a lower Ω_m to fit the observed D_V/r_d and F_{AP}. Figure 2 also illustrates the effect of dynamical dark energy leading to the BAO preference (lower χ^2) for higher H_0 values in ΛCDM, as the curve with a slightly higher $H_0 = 68.4$ has the smallest $\chi^2 = 0.2$.

3.2. Realizations from Posterior Samples of w_0w_aCDM

In this section we compare the amount of disagreement between real data probes analyzed individually in ΛCDM with the expected disagreement from mocks simulated in all viable w_0w_aCDM cosmologies to determine whether the real observed disagreement can be entirely explained by w_0w_aCDM. To ensure that the constraints on Ω_m shown in Figure 1 and the second row of Table 2 are not statistical flukes and to evaluate the probability of observing each Ω_m individually, we utilize the posterior DES24 chains provided[9] in DESI Collaboration (2024) for the w_0w_aCDM model. Specifically, we use the combined probe constraints (DES24) in w_0w_aCDM. For each set of cosmological parameters $\{w_0,\ w_a,\ \Omega_m,\ H_0\}$ from the DES24 chains, we generate mock SN, BAO, and CMB data sets with the methods described in Section 2, setting $\Omega_b h^2 = 0.02218$, the central value from BBN (V. Mossa et al. 2020), for CMB and BAO mock data sets. All three probes are simulated in the same w_0w_a cosmology. Each probe is then analyzed individually within the ΛCDM framework, treating both H_0 and Ω_m as free parameters.

The likelihood is maximized to find the best-fit values of Ω_m and H_0 for each of the SN, BAO, and CMB data sets generated in w_0w_aCDM. Although our mock SN data sets are not sensitive to H_0, we nonetheless float it simultaneously with Ω_m to match the methodology of DESI Collaboration (2024). Because this maximum likelihood is calculated thousands of times for each of the cosmologies in the DES24 chains, we simply calculate the maximum likelihood point and then compute the Hessian matrix ($\boldsymbol{H}$) at the best-fit values to estimate the uncertainties in Ω_m and H_0 as

$$\boldsymbol{H} = \begin{pmatrix} \dfrac{\partial^2(-\ln\mathcal{L})}{\partial\Omega_m^2} & \dfrac{\partial^2(-\ln\mathcal{L})}{\partial\Omega_m\partial H_0} \\ \dfrac{\partial^2(-\ln\mathcal{L})}{\partial H_0\partial\Omega_m} & \dfrac{\partial^2(-\ln\mathcal{L})}{\partial H_0^2} \end{pmatrix},$$

$$\sigma_{\Omega_m} = \sqrt{(\boldsymbol{H}^{-1})_{11}}$$
$$\sigma_{H_0} = \sqrt{(\boldsymbol{H}^{-1})_{22}}. \quad (12)$$

Finally, to build a probability distribution for the ΛCDM fits, we assume that each of the free parameters follows a Gaussian distribution $P^i(\Omega_{m,\mathrm{probe}}^{\Lambda\mathrm{CDM},i})$ for every background w_0w_aCDM cosmology i. These probabilities are then summed to produce the posterior density of ΛCDM parameters $P(\Omega_{m,\mathrm{probe}}^{\Lambda\mathrm{CDM}})$, given all of the background cosmologies from the DES24 chains. This process is mirrored to build the posterior probabilities $P(H_{0,\mathrm{probe}}^{\Lambda\mathrm{CDM}})$ for the Hubble constant H_0.

To quantify the statistical significance of the discrepancies in Ω_m among the probes, we perform a χ^2 test for consistency. For each set of Ω_m values obtained from the ΛCDM fits to the mock data sets, we calculate a χ^2 statistic for the fit under the assumption that all of the individual probes' measurements i are a random statistical fluctuation of a single $\Omega_{m,\mathrm{True}} = \frac{\sum_i \Omega_{m,i}/\sigma_i^2}{\sum_i 1/\sigma_i^2}$. We then quantify the probability that all

[9] At the time of this work, the DESI chains are not yet public.

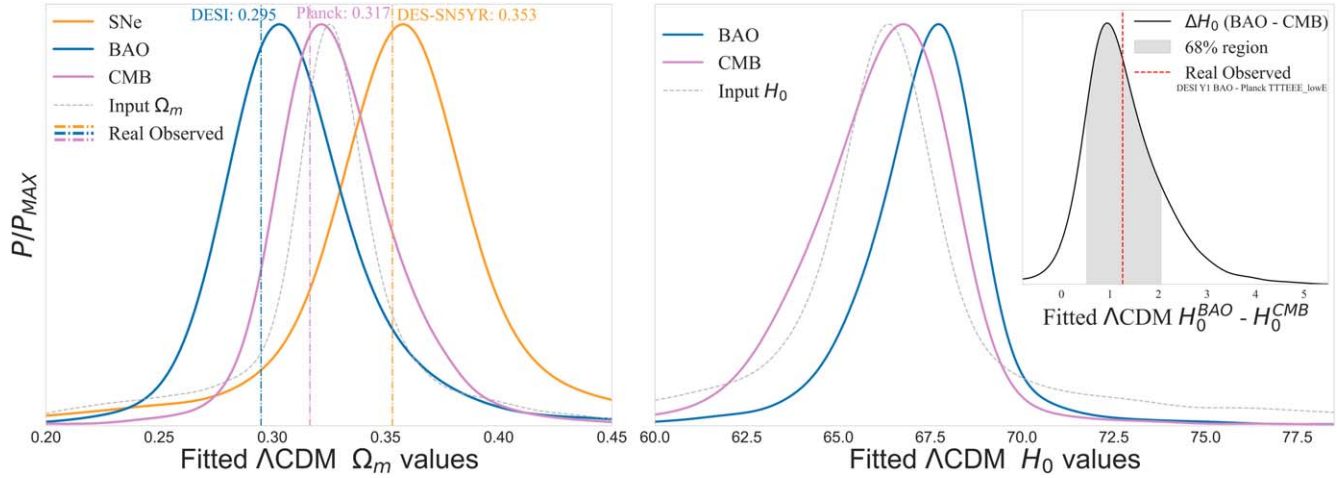

Figure 3. The figure shows marginalized ΛCDM fits for H_0 and Ω_m to mock data sets in w_0w_aCDM cosmologies. Simulated w_0w_aCDM sample the public DES24 chains. Left panel: the ΛCDMΩ_m distributions for various probes {SN, BAO, and CMB}. The gray dashed curve shows the underlying values of Ω_m used for these simulations. The three vertical lines represent the observed ΛCDMΩ_m values for real data for reference: DESI Y1 (DESI Collaboration 2025; blue), DES-SN 5YR (DESI Collaboration 2024; yellow), and Planck18 CMB only (Planck Collaboration 2020; pink). Right panel: the ΛCDMH_0 distributions for BAO and CMB probes. The gray dashed curve shows the w_0w_aCDMH_0 values used to simulate the mocks. SNe are not shown here because DES-like SNe are not sensitive to H_0 by themselves but require an external calibration. Right panel inset: the corresponding ΔH_0 distribution, quantifying the difference between H_0 results from BAO and CMB data sets at each step in the chains. The shaded region represents the 68% credible interval. The red dashed line indicates the observed ΔH_0 between DESI Y1 BAO and Planck18 CMB under ΛCDM. Our observed difference between the simulated w_0w_aCDM maximum likelihood H_0 and the "observed" mock-BAO ΛCDM maximum likelihood H_0 is 1.2 km s^{-1} Mpc^{-1}.

probes measure the same true $\Omega_{m,\mathrm{True}}$, i.e., the probability of obtaining a χ^2 value as extreme as or more extreme than the observed $\chi^2\dagger$ under the null hypothesis that all probes measure the same true $\Omega_{m,\mathrm{True}}$. This is given by $\chi^2\dagger = \sum_i \frac{(\Omega_{m,i} - \Omega_{m,\mathrm{True}})^2}{\sigma_i^2}$. We then compute the p-value using the χ^2 cumulative distribution function with $\nu = 2$ degrees of freedom,

$$p\text{-value} = 1 - \mathrm{CDF}_{\chi^2}(\chi^2\dagger, \nu). \quad (13)$$

A smaller p-value indicates that the discrepancies among the probes are less likely to occur by chance.

Using the best-fit Ω_m values and uncertainties reported by DES-SN 5YR $\Omega_m = 0.353 \pm 0.017$ (DESI Collaboration 2024), DESI Y1 BAO $\Omega_m = 0.295 \pm 0.015$ (DESI Collaboration 2025), and Planck 2018 CMB $\Omega_m = 0.315 \pm 0.007$ (Planck Collaboration 2020), the observed p-value is 0.035, shown in Table 2. In a frequentist sense, this means that if these three measurements with given uncertainties were all drawn from a single true value of Ω_m under ΛCDM, only about 3.5% of random realizations would exhibit discrepancies as large as or larger than what is observed. Also note that p-value = 0.013 if we calculate using the DESI Y1 full-shape analysis (DESI Collaboration 2025a) $\Omega_m = 0.2962 \pm 0.0095$ instead of the DESI Y1 BAO (DESI Collaboration 2025).

3.3. Results

3.3.1. Matter Density Ω

Our analysis reveals that the best-fit Ω_m values obtained from individual ΛCDM fits to the mock data sets differ across the probes when the true underlying cosmology is a dynamical dark energy. These Ω_m values are also observed in real data (DESI Collaboration 2025). As shown in Table 2, row 4 (DES-SN 5YR+CMB+BAO+3x2pt w_0w_a chains), the mock-BAO data prefer a lower Ω_m, the mock CMB data yield an intermediate Ω_m, and the mock SN data favor a higher Ω_m. The observed values from DESI Y1 BAO (DESI Collaboration 2025), Planck 2018 CMB (Planck Collaboration 2020), and DES-SN 5YR (DESI Collaboration 2024) are also shown in Figure 3 with vertical dashed–dotted lines for reference (also in Table 2, row 1). Our simulated Ω_m distributions closely match the observed values: the BAO Ω_m distribution peaks around 0.313, similar to the real DESI observed value of 0.295; the CMB Ω_m distribution centers around 0.323, matching the real Planck value of 0.317; and the SN Ω_m distribution peaks near 0.355, consistent with the real DES-SN 5YR value of 0.353.

To quantify the statistical significance of the discrepancies in ΛCDMΩ_m among the probes, we performed a p-value test for consistency as described in Section 3.1 with Equation (13), summarized in Table 2. For real data, the observed agreement between Ω_m has a p-value of 0.035 using DESI 2024 VI (DESI Collaboration 2025). With the release of DESI full-shape results, this discrepancy persists (DESI Collaboration 2025a), the p-value dropping to 0.013, showing an even larger discrepancy.

For mock data simulated in the DESI Collaboration (2025) best-fit w_0w_aCDM cosmology, we find a p-value of 0.003. When examining the distributions of ΛCDMΩ_m agreement p-values for all of the w_0w_aCDM cosmologies in the DES24 chains, we find that approximately 50.3% of the simulated w_0w_aCDM cosmologies have p-values smaller than that of the real observed data p-value <0.035 and that the 68% p-value confidence interval is [9×10^{-6}, 0.17]. Only 3.1% of the simulated cosmologies have $p > 0.5$. This suggests that if the true underlying w_0w_aCDM cosmology is indeed well characterized by DES24 w_0w_aCDM posteriors, the observed discrepancy in Ω_m in ΛCDM for the real data sets is entirely likely.

We also show a null test in the second row of Table 2, where ΛCDM is both the underlying mock cosmology and the assumed cosmology when fitting parameters, and we find agreement between the Ω_m values and corresponding p-value of 0.999.

3.3.2. Hubble Constant

Additionally, because we also simultaneously simulate H_0 in the mock data sets following each H_0 in the DES24 w_0w_aCDM chains, we can compare the fitted H_0 for BAO and CMB in ΛCDM. The best-fit values of H_0 derived from the BAO data are biased higher than the input and the CMB, as shown in Figure 3. The last row of Table 2 shows that our ΛCDM BAO results peak at $H_{0,\mathrm{BAO}}^{\Lambda\mathrm{CDM}} = 67.7\ \mathrm{km\ s^{-1}Mpc^{-1}}$, whereas for CMB we recover the input $H_{0,\mathrm{CMB}}^{\Lambda\mathrm{CDM}} = 66.7\ \mathrm{km\ s^{-1}Mpc^{-1}}$. The background simulated H_0 from the DES24 w_0w_aCDM chains have a mean of 66.4 km s^{-1} Mpc^{-1} (shown by the gray dashed vertical line in Figure 3). This trend of $\Delta H_0 \sim 1.2\ \mathrm{km\ s^{-1}\ Mpc^{-1}}$ is consistent with the findings reported in the DESI Collaboration's Year 1 results (DESI Collaboration 2025; also shown in the first row of Table 2), where BAO measurements indicate a higher value of the Hubble constant (∼68.5 km s^{-1} Mpc^{-1}) than those derived from Planck Collaboration (2020; ∼67 km s^{-1} Mpc^{-1}).

4. Discussion

This Letter set out to investigate whether an underlying dynamical dark energy cosmology could naturally produce the observed differences in Ω_m when data are analyzed under the ΛCDM framework. Using posterior samples from the chains of the DES Y5 cosmology analysis (DESI Collaboration 2024; to be updated to DESI Y1 when made publicly available), we generated mock data sets based on w_0w_aCDM cosmologies and then individually fit the various probes with a ΛCDM model. We found that the differences in the best-fit Ω_m values between SN, BAO, and CMB data sets closely match the discrepancies observed in real data.

These results suggest that the observed discrepancies in Ω_m in ΛCDM between different probes can indeed be explained by an evolving dark energy model. However, we show in Appendix A that we cannot rule out the inverse possibility that unknown systematic errors that mimic differences in Ω_m in ΛCDM could be the source of the dynamical dark energy signal. It is thus extremely important to understand whether the differences between the probes on Ω_m could be systematically driven.

The current state-of-the-art analyses of SNe (Pantheon+, D. Brout et al. 2022a; DES-SN 5YR, DESI Collaboration 2024; Union3, D. Rubin et al. 2023) are consistent with high Ω_m. It is important to note that while the DES and Pantheon+ samples are largely independent, they do share many of the low-z SNe. And while the Pantheon+ and Union3 samples utilize vastly different cosmological pipelines (one frequentist validated P. Armstrong et al. 2023, another hierarchical Bayesian D. Rubin et al. 2015), they share many of the same SNe and the underlying SALT model (W. D. Kenworthy et al. 2021). Therefore, while there is agreement between the three samples toward higher Ω_m, there is the possibility of correlated or common systematics. Conversely, D. Brout et al. (2022a, Appendix Figure 15) highlight the major updates that have occurred in the past decade of SN cosmology that have contributed to higher Ω_m. There are roughly equal contributions from (1) updating the Milky Way dust color law from Cardelli, Clayton, and Mathis (J. A. Cardelli et al. 1989) to Fitzpatrick (E. L. Fitzpatrick 1999), (2) updating the SALT2 model (G. Taylor et al. 2021) to include the modern calibrations (D. Brout et al. 2022b; E. S. Rykoff et al. 2023), and (3) updating from a color-independent SN intrinsic scatter model (D. Brout & D. Scolnic 2021; B. Popovic et al. 2023) to a color- and dust-dependent physically motivated model. These updates were introduced to improve treatment of the largest sources of systematics in SN cosmology (Milky Way extinction, light-curve calibration and fitting, and SN Ia intrinsic scatter modeling; D. Brout et al. 2022a; M. Vincenzi et al. 2024; D. Rubin et al. 2023) and constitute an objective improvement to previous SN analyses. Uncertainties in the updates themselves remain accounted for in the reported systematic uncertainties.

The BAO-derived value of ΛCDMΩ_m from DESI Y1 (DESI Collaboration 2025) is slightly lower than that obtained from Planck CMB (Planck Collaboration 2020) and SN (DESI Collaboration 2024; D. Brout et al. 2022a; D. Rubin et al. 2023) observations. The DESI Year 1 BAO analysis includes thorough evaluations of theoretical modeling uncertainties (estimated to be at most 0.1%–0.2% of the BAO parameters), uncertainties due to the galaxy–halo connection (less than 0.2%), and observational systematic effects, which are found to be negligible. These updates were introduced to improve the treatment of the largest sources of systematics in BAO cosmology and represent objective improvements over previous analyses. Since the systematic contributions are significantly smaller than the statistical uncertainties, unaccounted-for systematics remain unlikely, as they would have to be an order of magnitude larger than the current best-known systematics to be the cause of the slightly low Ω_m inferred from BAO. While the observed discrepancy between BAO and CMB is very small (∼1.2σ), it could simply be due to statistical fluctuations or sample/cosmic variance.

An interesting outcome of this work is that we find that for the BAO mock data sets in w_0w_aCDM background cosmologies, when analyzed under the ΛCDM model, the BAO data exhibit a preference for a slightly higher value of the Hubble constant $\Delta H_0 = 1.2\ \mathrm{km\ s^{-1}\ Mpc^{-1}}$ than predicted by the CMB. Inconsistencies between CMB and BAO predicted values for H0 are expected if the modeled late-time cosmology is different from the true underlying physics. This tendency of BAO data to favor a higher H_0 qualitatively aligns with the findings from the DESI Year 1 results (DESI Collaboration 2025), where BAO measurements indicate a Hubble constant around ∼67.62 km s^{-1} Mpc^{-1}, in contrast to the lower value of ∼66.6 km s^{-1} Mpc^{-1} derived from the mock Planck CMB data (Planck Collaboration 2020).

Cumulatively, our results do support the possibility that an underlying dynamical dark energy model could be responsible for the observed discrepancies. This is consistent with the findings of K. V. Berghaus et al. (2024), who showed that scalar field models with nonnegligible kinetic energy can alleviate tensions between SN and BAO data sets. Y. Tada & T. Terada (2024) further explored quintessential dark energy models in light of DESI observations, suggesting that such models can provide better fits to the data. In addition, we have tested the robustness of these conclusions and checked for prior-volume effects using a profile likelihood analysis (see Appendix F), confirming that they hold even when exploring potential non-Gaussian behaviors in the w_0w_a parameter space.

However, it is important to acknowledge the limitations of our study. Our simulations used idealized data sets without observational noise or scatter, focusing on the impact of cosmological models without the complications introduced by

statistical fluctuations. While this simplification allows us to isolate and clearly demonstrate how discrepancies in Ω_m and H_0 are related to the signal of dynamical dark energy, it does not capture the full complexity of real observational data. In practice, data sets are subject to various sources of uncertainty, including measurement errors, selection effects, calibration issues, and physics systematics, which can influence parameter estimation. Moreover, for the CMB analysis, we relied on compressed CMB parameters—the shift parameter R and the acoustic scale l_A, with uncertainties derived from Planck 2018 results under the ΛCDM model. While R and l_A are designed to be model-independent compressions relevant for dark energy studies, their uncertainties can be model dependent, especially when extending beyond ΛCDM to models like w_0w_aCDM. For the BAO and CMB analyses, due to concerns with the minimization procedure, we fixed $\Omega_b h^2$ to its central value from BBN (V. Mossa et al. 2020), complicating its uncertainty and the potential Gaussianity assumption in the Hessian matrix maximization analysis. One caveat is that simplification may not accurately reflect the true uncertainties in the BAO and CMB constraints, and we do take a Gaussian prior into account for our MCMC analysis.

In conclusion, the observed discrepancies in Ω_m between SN, BAO, and CMB data sets and in H_0 between BAO and CMB can be explained simultaneously by a dynamical dark energy model. This underscores the necessity for meticulous analysis methods and the careful consideration of systematic uncertainties in cosmological research. As upcoming analyses (DES Y6 weak lensing and galaxy clustering, DESI Y3/Y5) and future surveys like the Vera C. Rubin Observatory's LSST and the Euclid mission provide more precise data about background expansion and structure formation, we will soon learn the extent of the significance of the w_0w_a signal and whether the growth of structure is also compatible with dynamical dark energy.

Acknowledgments

We thank Licia Verde, Sesh Nadathur, Adam Riess, Daniel Scolnic, Dragan Huterer, and Tamara Davis for their commentary. We also thank Hongwan Liu, Martin Schmaltz, and Nickolas Kokron for extended useful conversations.

We thank the Templeton Foundation for directly supporting this research.

All simulations and calculations were performed using Python and several scientific computing packages. The `Astropy` package (T. P. Robitaille et al. 2013) was used for cosmological computations, such as distance calculations and model evaluations. Numerical computations were carried out using `NumPy` (C. R. Harris et al. 2020), and `SciPy` (P. Virtanen et al. 2020) was used for integration and optimization. The MCMC analyses utilized the `emcee` package (D. Foreman-Mackey et al. 2013). We use `matplotlib`, `corner` (D. Foreman-Mackey et al. 2016) and `Chainconsumer` (S. R. Hinton 2016) for plotting.

Appendix A
False Signal from Discrepancies Purely in ΛCDM?

If each data set is consistent with ΛCDM alone, but they are inconsistent with each other (in Ω_m and H_0), could combining them in a joint analysis lead to a false detection of evolving dark energy? Such Ω_m and H_0 discrepancies could be due to fluctuations in the data (either statistical or systematic) that result in the data best matching different central values.

To address this question to first order, we explicitly simulate each data set in a ΛCDM cosmology, but with different Ω_m and H_0 to mimic either a statistical or systematic fluctuation. It is important to note that this methodology oversimplifies the impact of both statistical fluctuations and systematic errors within one probe, and we leave a more realistic analysis for future work. Following Section 2, we simulate SN, BAO, and CMB data sets under the ΛCDM model but with different values of Ω_m for each probe, consistent with what is observed in real data for each probe individually (DESI Collaboration 2025; DESI Collaboration 2024; Planck Collaboration 2020). Similarly, we simultaneously simulate CMB and BAO with different values of H_0. We note that because the SN likelihood includes absolute magnitude M as an unconstrained variable, the results in this section are insensitive to the value of H_0 chosen for the SN mocks. The explicit cosmologies simulated for each probe are

$$\text{SNeMock: } \Lambda\text{CDM}, \Omega_m = 0.353$$

$$\text{BAOMock: } \Lambda\text{CDM}, \Omega_m = 0.295, \ H_0 = 68.5 \text{ km s}^{-1} \text{ Mpc}^{-1}$$

$$\text{CMBMock: } \Lambda\text{CDM}, \Omega_m = 0.315, \quad H_0 = 67.3 \text{ km s}^{-1} \text{ Mpc}^{-1}.$$

We then perform an MCMC analysis on the combined data sets with log-likelihood

$$\ln \mathcal{L}_{\text{combined}} = \ln \mathcal{L}_{\text{SNe}} + \ln \mathcal{L}_{\text{BAO}} + \ln \mathcal{L}_{\text{CMB}}, \tag{A1}$$

where the likelihood of each probe is calculated from Equations (3), (8), and (10). We then fit them jointly to a w_0w_aCDM model to see whether the discrepancies in Ω_m lead to apparent signals of evolving dark energy and derive constraints on Ω_m, H_0, w_0, and w_a from the combination of simulated data sets.

A.1. Results from ΛCDM$\Omega_{\rm m}$ Discrepancies

Analyzing the combined simulated data sets generated under ΛCDM and fitted under the w_0w_aCDM model, we find the following constraints when combining only SNe ($\Omega_m = 0.353$) and BAO ($\Omega_m = 0.295$, $H_0 = 68.5$ km s^{-1} Mpc^{-1}):

$$w_0 = -0.856^{+0.054}_{-0.066}, \quad w_a = 0.16^{+0.57}_{-0.50}.$$

These results are shown by the purple contour in Figure 4. We observe that w_a is consistent with zero within uncertainties and $w_0 \approx -0.86$, indicating no significant deviation from the ΛCDM model.

Next, we analyze the combination of BAO ($\Omega_m = 0.295$, $H_0 = 68.5$ km s^{-1} Mpc^{-1}) and CMB ($\Omega_m = 0.315$, $H_0 = 67.3$ km s^{-1} Mpc^{-1}) mock data sets and obtain

$$w_0 = -0.70^{+0.37}_{-0.40}, \quad w_a = -0.66^{+0.79}_{-1.38}.$$

These results are represented by the gray contour in Figure 4. The central value of $w_0 = -0.70$ is less negative than the ΛCDM value of -1 but consistent within uncertainties with ΛCDM. Similarly, the central value $w_a = -0.66$ suggests a mild preference for evolving dark energy, but the large uncertainties make it consistent with zero.

When all the mock data sets are combined—SNe ($\Omega_m = 0.353$), BAO ($\Omega_m = 0.295$, $H_0 = 68.5$ km s^{-1} Mpc^{-1}),

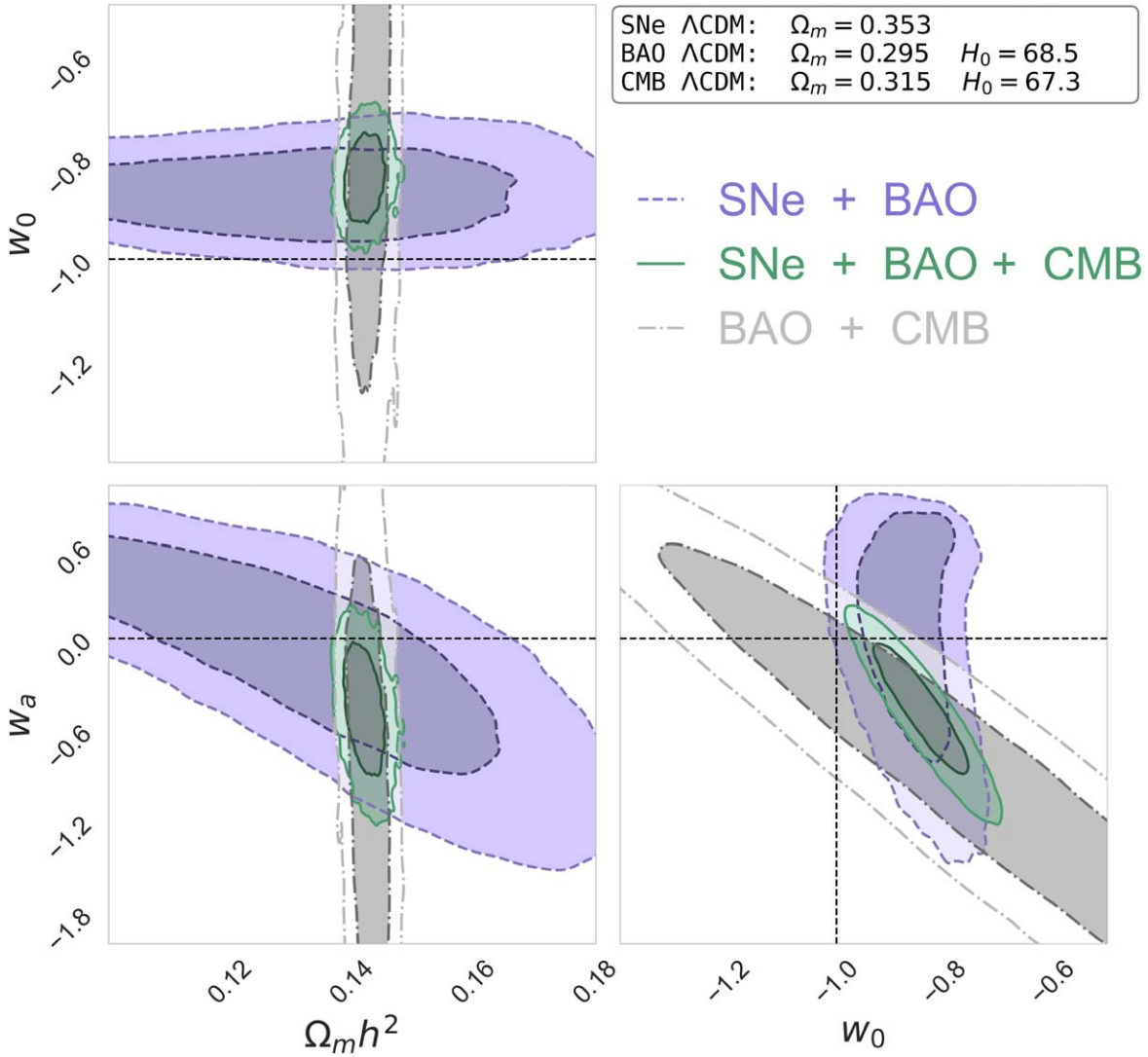

Figure 4. MCMC results testing the w_0w_aCDM model using mock data combined from different probe-like data sets generated under the ΛCDM model but with different Ω_m and H_0. The black dashed lines indicate the ΛCDM values ($w_0 = -1$, $w_a = 0$). The purple contour represents the constraints from mock SN ($\Omega_m = 0.353$) and BAO ($\Omega_m = 0.295$, $H_0 = 68.5$ km s^{-1} Mpc^{-1}) data. The green contour adds the CMB ($\Omega_m = 0.315$, $H_0 = 67.3$ km s^{-1} Mpc^{-1}) mock data to the previous combination. The gray contour shows the constraints from BAO and CMB mock data. This figure illustrates how discrepancies in the ΛCDM model's Ω_m and H_0 among different data sets can lead to signals of dynamical dark energy when analyzed under the w_0w_aCDM model.

and CMB ($\Omega_m = 0.315$, $H_0 = 67.3$ km s^{-1} Mpc^{-1})—we find

$$w_0 = -0.851^{+0.065}_{-0.050}, \quad w_a = -0.44^{+0.27}_{-0.30}.$$

These results are shown by the green contour in Figure 4. The preferences for $w_a < 0$ and a more positive $w_0 \approx -0.85$ become more pronounced, reaching levels of approximately 2.6σ for w_0 and 1.5σ for w_a. These values suggest that discrepancies in Ω_m and H_0 in the ΛCDM model between different data sets can lead to apparent deviations from ΛCDM when analyzed under the w_0w_aCDM framework, even though each data set was originally simulated in a ΛCDM universe.

In contrast, when only Ω_m discrepancies are present (and H_0 is consistent across data sets), combining all mock data sets gives results that are consistent with ΛCDM values of w_0 and w_a within 1σ. This suggests that in order to mimic a dynamical dark energy signal in a universe that is truly ΛCDM, systematic effects need to produce discrepancies in both Ω_m and H_0 among different data sets. Such combined discrepancies can lead to apparent preferences for evolving dark energy when analyzing the data under the w_0w_aCDM framework.

Comparing these results to those observed in the DESI Year 1 combined-probes analysis (DESI Collaboration 2025) indicates that discrepancies in Ω_m and H_0 can induce apparent deviations from ΛCDM, and the significance of these deviations depends on the magnitude of the discrepancies and the precision of the data sets involved.

Appendix B
Grid-based Chain-independent Exploration

So far, we have demonstrated that viable w_0w_aCDM cosmologies, as constrained by DES24, tend to result in different Ω_m when constrained in ΛCDM, similar to those observed in real data. In this appendix, we aim to present a uniform approach to determining the set of w_0w_aCDM cosmologies that produce ΛCDMΩ_m differences among probes comparable to those observed in read data. By definition, this

set will encompass parameter volumes as large as, or larger than, those supported by the DES24 constraints.

We perform a grid-based exploration of the w_0w_a parameter space. This approach is independent of specific MCMC chains and allows us to identify regions where the observed discrepancies in Ω_m can be reproduced. We construct a grid over a range of $\{w_0, w_a, \Omega_m\}$ values, covering $w_0 \in [-1.2, 0.1]$, $w_a \in [-6, 1]$, and $\Omega_m \in [0.23, 0.4]$. For each grid point (w_0, w_a, Ω_m), we generate mock data sets for SNe, BAO, and CMB using the methods described in Section 2. For each mock data set, we find the ΛCDM best-fit Ω_m (as well as H_0) values for each probe individually. We seek to compare these fitted Ω_m values to the observed values from real data:

1. DES-SN 5YR: $\Omega_{m,\mathrm{obs}}^{\mathrm{SNe}} = 0.353 \pm 0.017$ (DESI Collaboration 2024);
2. DESI BAO: $\Omega_{m,\mathrm{obs}}^{\mathrm{BAO}} = 0.295 \pm 0.015$ (DESI Collaboration 2025);
3. Planck 2018 CMB: $\Omega_{m,\mathrm{obs}}^{\mathrm{CMB}} = 0.315 \pm 0.007$ (Planck Collaboration 2020).

Quantitatively, we compute the likelihood of the best-fit Ω_m values being consistent with the observed values for each probe using the Gaussian probability density function

$$\mathcal{L}^*_{\mathrm{probe}} = \exp\left(-\frac{(\Omega_{m,\mathrm{fit}} - \Omega_{m,\mathrm{obs}})^2}{2\sigma^2_{\mathrm{obs}}}\right), \tag{B1}$$

where $\Omega_{m,\mathrm{fit}}$ is the best-fit value from the ΛCDM analysis of the mock data and σ_{obs} is the observed uncertainty. The joint likelihood for each grid point was calculated by multiplying the likelihoods from all three probes

$$\mathcal{L}^*_{\mathrm{joint}} = \mathcal{L}^*_{\mathrm{SNe}} \times \mathcal{L}^*_{\mathrm{BAO}} \times \mathcal{L}^*_{\mathrm{CMB}}. \tag{B2}$$

To visualize the results and compare them with observational data, we employ the `ChainConsumer` package (S. R. Hinton 2016). We create a data set containing the grid points (w_0, w_a, Ω_m) and their corresponding joint likelihoods. The weights were calculated as described by Equation (B2) and normalized. We also include posterior samples from the combined DES24 w_0w_aCDM chain (DESI Collaboration 2024) for comparison.

The results of our grid-based exploration are summarized in contour plots in Figure 5. The blue contours represent regions where the best-fit Ω_m values from each probe's ΛCDM analysis align with the observed Ω_m values. Hence, these contours

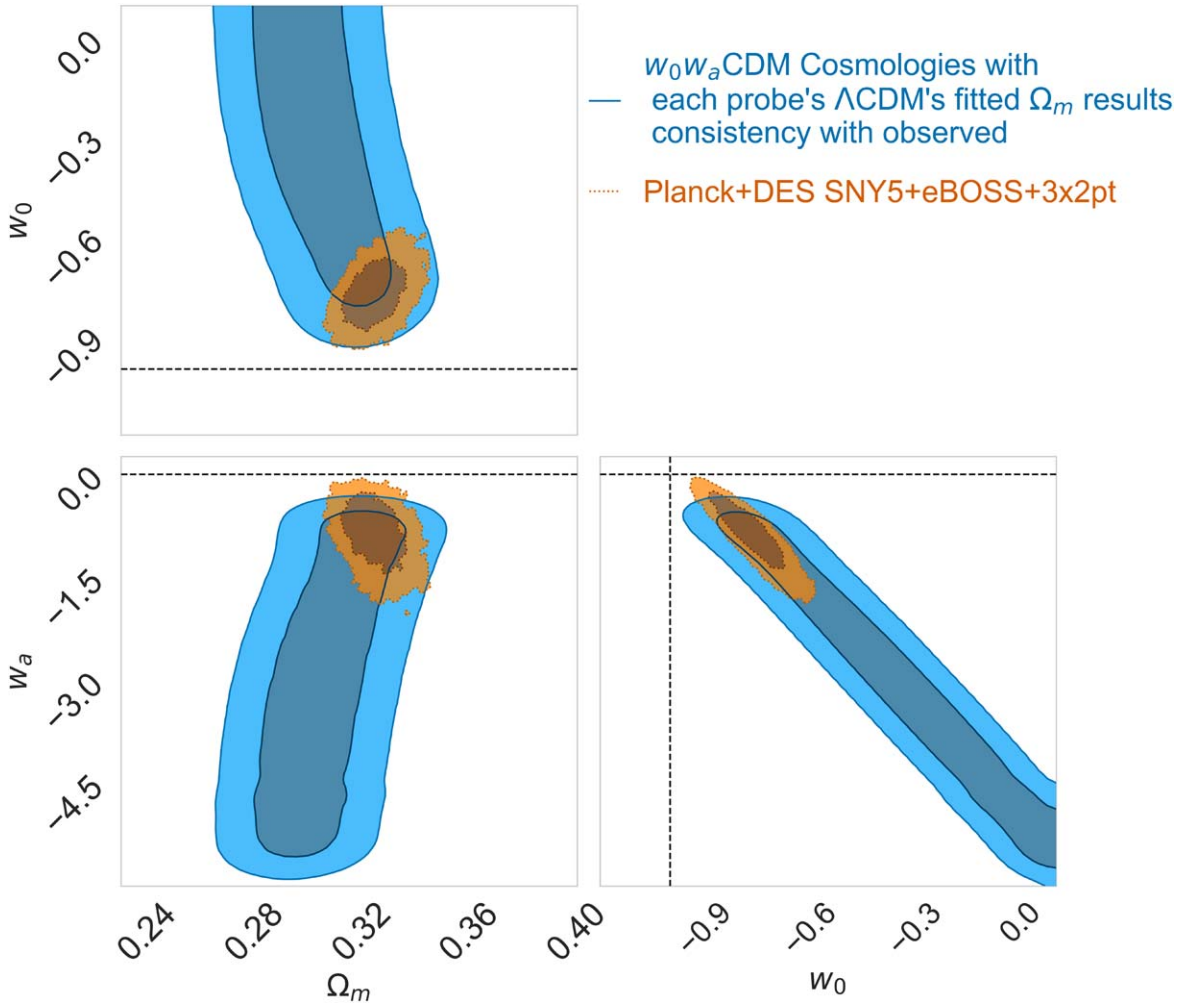

Figure 5. Results of the grid-based exploration of the w_0w_a parameter space that can generate the observed discrepancies in ΛCDMΩ_m. Blue contours represent grid points where each probe's fitted ΛCDMΩ_m values are similar to observed values (which are 0.353 ± 0.017 for SNe, 0.295 ± 0.015 for BAO, and 0.315 ± 0.007 for CMB; DESI Collaboration 2024; DESI Collaboration 2025; Planck Collaboration 2020), with the 1σ and 2σ contours obtained from the likelihood $\mathcal{L}^*_{\mathrm{joint}}$ from Equation (B2). The orange contours show the samples from the DES24 chain (DESI Collaboration 2024). Black dashed lines indicate ΛCDM values ($w_0 = -1$, $w_a = 0$).

effectively highlight regions in the w_0w_a parameter space where each simulated probe individually produces a $\Lambda\mathrm{CDM}\Omega_m$ result consistent with its real observational counterpart. The orange contours, on the other hand, show the posterior distribution of w_0 and w_a from a combined analysis of DES24 data (DESI Collaboration 2024). The orange DES24 constraints are largely aligned with, and a subset of, our blue grid-based exploration; however, we note that there exist many more combinations of cosmological parameters that can reconcile the discrepant $\Lambda\mathrm{CDM}\Omega_m$ values (as evidenced by the larger extent of the blue contour).

Appendix C
Impact of Direct Calibration of the Sound Horizon r_d

In our main analysis, as stated in Section 2, the BAO data were used with a model-dependent computation of the sound horizon r_d at the drag epoch, which depends on cosmological parameters such as $\Omega_m h^2$ and $\Omega_b h^2$. Specifically, we used the scaling relation from Equation (2.5) in the DESI Y1 paper (DESI Collaboration 2025) and BBN in our main analysis. We note that the r_d constraints we applied are from a Planck ΛCDM fit. In this section, we use mock data simulated in w_0w_aCDM cosmologies and then fit them assuming ΛCDM. The r_d constraints might therefore be less reliable here because we are simulating in w_0w_aCDM cosmologies. The direct r_d calibration was included here to maintain consistency with the ΛCDM fit in the DESI Y1 BAO analysis (DESI Collaboration 2025).

Closely following the methodology used by the DESI Collaboration in their Year 1 results (DESI Collaboration 2025), we explore the impact of directly calibrating r_d using external constraints. Specifically, we adopt a Gaussian prior on r_d based on CMB measurements,

$$r_d = 147.09 \pm 0.26 \quad \mathrm{Mpc}. \tag{C1}$$

This direct calibration effectively decouples r_d from the late-time cosmological parameters, thereby breaking the degeneracy between H_0 and r_d inherent in BAO measurements when r_d is computed from the cosmological model.

We modify our BAO analysis by directly calibrating r_d. In practice, this means that, when computing the BAO observables, we treat r_d as an external parameter drawn from a Gaussian distribution with the mean and standard deviation specified above.

Constraints in the Ω_m–H_0 plane. Figure 6 (direct r_d calibrating version of Figure 1) shows the constraints on Ω_m and H_0 obtained by fitting the ΛCDM model to mock data sets generated in the DESI Y1 best-fit w_0w_aCDM cosmology (DESI Collaboration 2025). With the direct r_d calibration, the BAO constraints become less circular as additional degeneracies open up in the Ω_m–H_0 plane compared to when only $\Omega_b h^2$ is provided (blue contours in Figures 1 and 6).

Hubble Constant Discrepancy. Despite the direct calibration of r_d, we still observe a discrepancy in the best-fit H_0 values when the true cosmology is w_0w_aCDM but data are analyzed under the ΛCDM model. Figure 7 illustrates that the BAO data prefer a higher H_0, consistent with our findings in the main text in Section 3.3 and Figure 3. The direct calibration of r_d has a slightly larger H_0 than taking a prior on $\Omega_b h^2$. The difference between the simulated w_0w_aCDM maximum likelihood H_0 and observed direct calibration of r_d with BAO in ΛCDM maximum likelihood H_0 grows to 1.67 km s^{-1} Mpc^{-1}, which is a slightly larger difference than when using the prior on $\Omega_b h^2$ (1.22 km s^{-1} Mpc^{-1}). This difference in inferred H_0 for r_d calibrated and using a prior on $\Omega_b h^2$ is quantitatively similar to DESI Y1's results in Equations (4.3) and (4.4) in DESI Collaboration (2025).

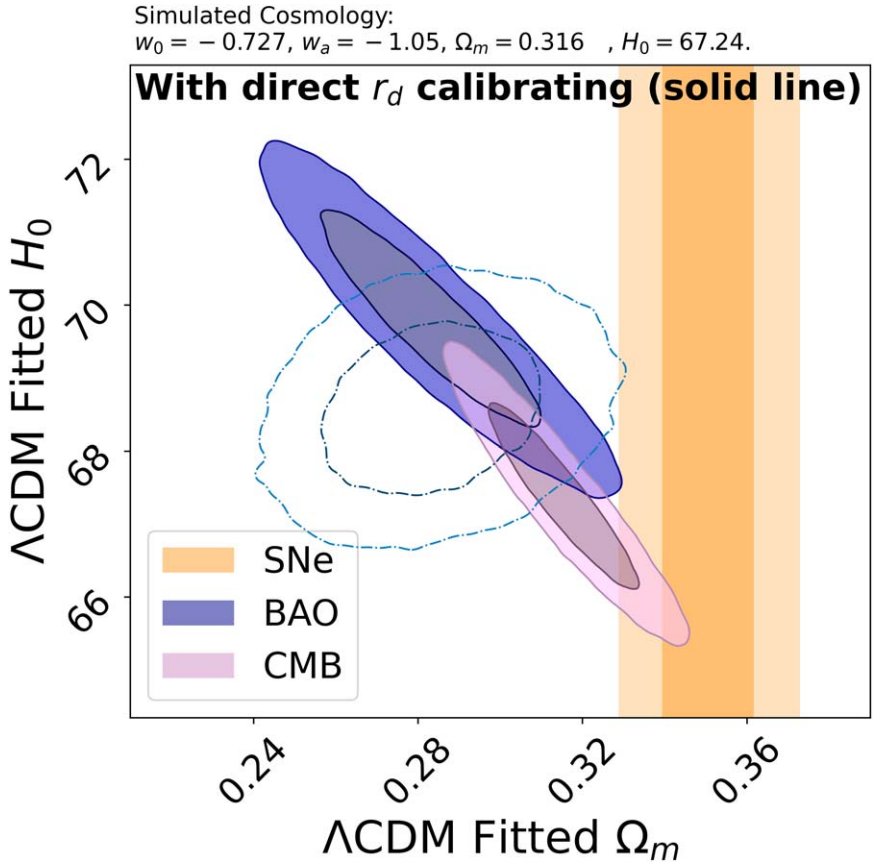

Figure 6. Constraints on Ω_m and H_0 obtained by fitting the ΛCDM model to mock CMB, BAO, and SN data sets generated in the best-fit w_0w_aCDM cosmology ($w_0 = -0.727$, $w_a = -1.05$, $\Omega_m = 0.316$, $H_0 = 67.24$ km s^{-1} Mpc^{-1}), with direct r_d calibration. The BAO constraints (dark blue contours) become less circular in the Ω_m–H_0 plane compared to the case without direct r_d calibration (Figure 1, also shown here as the dashed–dotted contours).

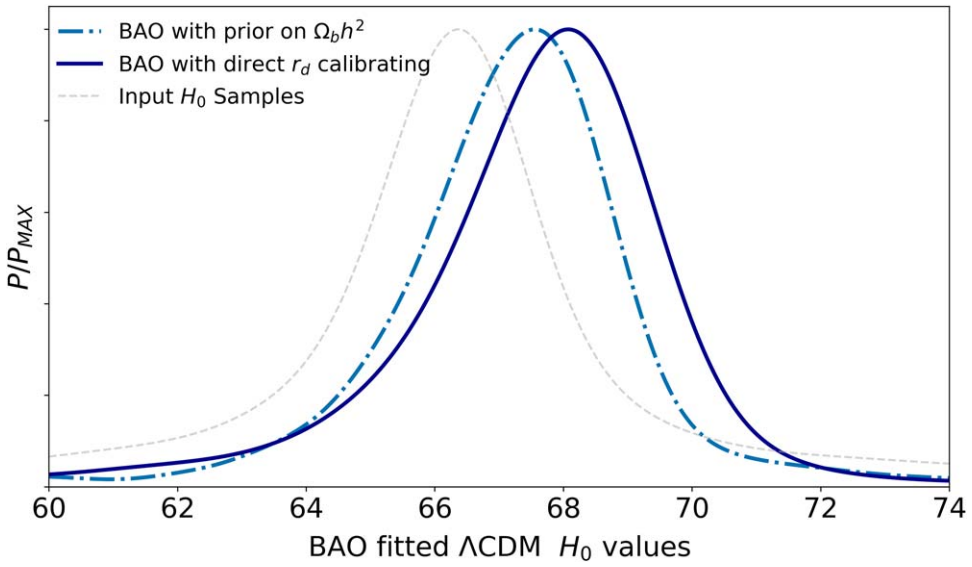

Figure 7. Probability distributions of the fitted H_0 values (in km s^{-1} Mpc^{-1}) from BAO under the ΛCDM model, with (blue solid line) and without (blue dashed–dotted line; same as the one in the main text, right panel of Figure 3) direct r_d calibration. The input H_0 values from the DES24 w_0w_aCDM background cosmologies are indicated by the gray dashed line. Both in the direct r_d calibration and using a prior on $\Omega_b h^2$, the BAO data prefer a higher H_0 than what was simulated.

Appendix D
Fisher Matrix Analysis

In this appendix, we perform a Fisher matrix analysis to quantify how sensitive our cosmological observables are to the parameters Ω_m and H_0. This analysis serves as a cross-check of the constraints derived from our mock data sets. Additionally, Fisher formalism provides a theoretical approach that allows for a simplified computation of parameter constraints, demonstrating how different probes—at various redshifts or precision levels—contribute to shaping the parameter space constraints, without relying on mock data.

The Hubble parameter is

$$E(z) = \sqrt{\Omega_m(1+z)^3 + (1-\Omega_m)(1+z)^{3(1+w_0+w_a)} e^{-\frac{3w_a z}{1+z}}}.$$

D.1. Fisher Matrix Construction

D.1.1. SN Fisher

The derivative of the SN data point is

$$\frac{\partial d_L(z)}{\partial \Omega_m} = (1+z)\frac{c}{H_0}\int_0^z \frac{-\frac{(1+z')^3-1}{2E(z')^3}}{E(z')} dz'.$$

The Fisher matrix $F^{\rm SNe}$ for SN data is

$$F^{\rm SNe} = \sum_{n,m=1}^{N} \frac{\partial \mu(z_n)}{\partial \Omega_m} [\boldsymbol{C}_{\rm DES}{}^{-1}]_{nm} \frac{\partial \mu(z_m)}{\partial \Omega_m},$$

where N is the number of SN data points.

While the derivative of the distance modulus $\mu(z)$ with respect to H_0 is theoretically meaningful, it is not included in our Fisher matrix analysis because the intrinsic absolute magnitude M of an SN is unknown. Without a precise calibration of M, SN data alone cannot constrain H_0. The degeneracy between M and H_0 in the distance modulus equation,

$$\mu(z) = 5\log_{10}[d_L(z)] + 25 - M,$$

renders H_0 effectively unconstrained without additional external calibration. As a result, our Fisher analysis for SNe focuses solely on constraints for Ω_m, assuming that H_0 remains degenerate with M.

D.1.2. BAO Fisher

The derivative of the BAO data point is

$$\frac{\partial D_V(z)}{\partial \Omega_m} = D_V(z)\left[\frac{2}{3}\frac{\frac{\partial I(z)}{\partial \Omega_m}}{I(z)} - \frac{1}{3}\frac{\frac{\partial E(z)}{\partial \Omega_m}}{E(z)}\right],$$

$$\frac{\partial D_V(z)}{\partial H_0} = -\frac{D_V(z)}{H_0};$$

$$\frac{\partial F_{\rm AP}(z)}{\partial \Omega_m} = \frac{\partial E(z)}{\partial \Omega_m}\cdot I(z) + E(z)\cdot\frac{\partial I(z)}{\partial \Omega_m},$$

$$\frac{\partial F_{\rm AP}(z)}{\partial H_0} = 0,$$

where $I(z) \equiv \int_0^z \frac{dz'}{E(z')}$ and $\frac{\partial I(z)}{\partial \Omega_m} = \int_0^z -\frac{1}{E(z')^2}\frac{\partial E(z')}{\partial \Omega_m} dz'$.

The Fisher matrix $F_{ij}^{\rm BAO}$ for BAO data is constructed by summing contributions from both $D_V(z)$ and $F_{\rm AP}(z)$ measurements:

$$F_{\rm BAO} = \sum_{k=1}^{N_{D_V}} \frac{1}{\sigma_{D_V,k}^2}\begin{pmatrix} \frac{\partial D_V(z_k)}{\partial \Omega_m} \\ \frac{\partial D_V(z_k)}{\partial H_0}\end{pmatrix}\begin{pmatrix} \frac{\partial D_V(z_k)}{\partial \Omega_m} & \frac{\partial D_V(z_k)}{\partial H_0}\end{pmatrix} + \sum_{l=1}^{N_{F_{\rm AP}}} \frac{1}{\sigma_{F_{\rm AP},l}^2}\begin{pmatrix} \frac{\partial F_{\rm AP}(z_l)}{\partial \Omega_m} \\ \frac{\partial F_{\rm AP}(z_l)}{\partial H_0}\end{pmatrix}\begin{pmatrix} \frac{\partial F_{\rm AP}(z_l)}{\partial \Omega_m} & \frac{\partial F_{\rm AP}(z_l)}{\partial H_0}\end{pmatrix}.$$

N_{D_V} and $N_{F_{\rm AP}}$ are the number of BAO data points for $D_V(z)$ and $F_{\rm AP}(z)$, respectively, and $\sigma_{D_V,k}$ and $\sigma_{F_{\rm AP},l}$ are the uncertainties associated with each measurement.

D.1.3. CMB Fisher

Due to the complexity of the analytical expressions for the derivatives of R and l_A with respect to the cosmological parameters, we compute these partial derivatives numerically using finite difference. Detailed analytical derivatives are available in our supplementary material:[10]

$$\boldsymbol{J}_{\rm CMB} = \begin{pmatrix} \frac{\partial R}{\partial \Omega_m} & \frac{\partial R}{\partial H_0} \\ \frac{\partial l_A}{\partial \Omega_m} & \frac{\partial l_A}{\partial H_0}\end{pmatrix}.$$

The Fisher matrix $\boldsymbol{F}_{\rm CMB}$ for the CMB data is constructed as

$$\boldsymbol{F}_{\rm CMB} = \boldsymbol{J}_{\rm CMB}^T \boldsymbol{C}_{\rm P18}^{-1} \boldsymbol{J}_{\rm CMB},$$

where $\boldsymbol{C}_{\rm P18}^{-1}$ is the inverse of the covariance matrix defined in Equation (9).

D.2. Parameter Estimation

The maximum likelihood estimates for the cosmological parameters are obtained by minimizing the Fisher matrix formalism for each data set. Each data set contributes its own Fisher matrix and Jacobian matrix, which are combined to derive joint constraints on the cosmological parameters Ω_m and H_0.

For SN data, the parameter shifts are defined as

$$\Delta\mu = \mu_{\rm fid} - \mu_{\Lambda\rm CDM},$$

$$\boldsymbol{\Omega_m}_{\rm ML}^{(\rm SNe)} = \boldsymbol{\Omega_m}_{\rm fid} + \boldsymbol{F}_{\rm SNe}^{-1}\boldsymbol{J}_{\rm SNe}^T\boldsymbol{C}_{\rm DES}^{-1}\Delta\mu.$$

The uncertainties in the parameters are given by the square roots of the diagonal elements of the inverse Fisher matrix:

$$\sigma_{\Omega_m}^{\rm SNe} = \sqrt{\boldsymbol{F}_{\rm SNe}^{-1}}.$$

For BAO data, the parameter shifts $\Delta\boldsymbol{\theta}_{\rm BAO}$ are computed as

$$\Delta\boldsymbol{\theta}_{\rm BAO} = \boldsymbol{F}_{\rm BAO}^{-1}\begin{pmatrix} \sum_{k=1}^{N_{D_V}} \frac{\frac{\partial D_V(z_k)}{\partial \Omega_m}\Delta{\rm BAO}_k}{\sigma_{D_V,k}^2} + \sum_{l=1}^{N_{F_{\rm AP}}} \frac{\frac{\partial F_{\rm AP}(z_l)}{\partial \Omega_m}\Delta{\rm BAO}_l}{\sigma_{F_{\rm AP},l}^2} \\ \sum_{k=1}^{N_{D_V}} \frac{\frac{\partial D_V(z_k)}{\partial H_0}\Delta{\rm BAO}_k}{\sigma_{D_V,k}^2}\end{pmatrix}.$$

Thus, the maximum likelihood estimates are

$$\boldsymbol{\theta}_{\rm ML}^{(\rm BAO)} = \boldsymbol{\theta}_{\rm fid} + \Delta\boldsymbol{\theta}_{\rm BAO},$$

with uncertainties

$$\sigma_{\Omega_m}^{\rm BAO} = \sqrt{(\boldsymbol{F}_{\rm BAO}^{-1})_{11}}, \quad \sigma_{H_0}^{\rm BAO} = \sqrt{(\boldsymbol{F}_{\rm BAO}^{-1})_{22}}.$$

For CMB data, the parameter shifts are computed as

$$\Delta_{\rm CMB} = \begin{pmatrix} R_{\Lambda\rm CDM} - R_{\rm fid} \\ l_{A,\Lambda\rm CDM} - l_{A,\rm fid}\end{pmatrix},$$

[10] Analytical derivatives of our CMB parameters can be found at https://github.com/trivialTZ/DM_DE_Signals_in_SNe_BAO_CMB/blob/main/Fisher_d_cmb.pdf.

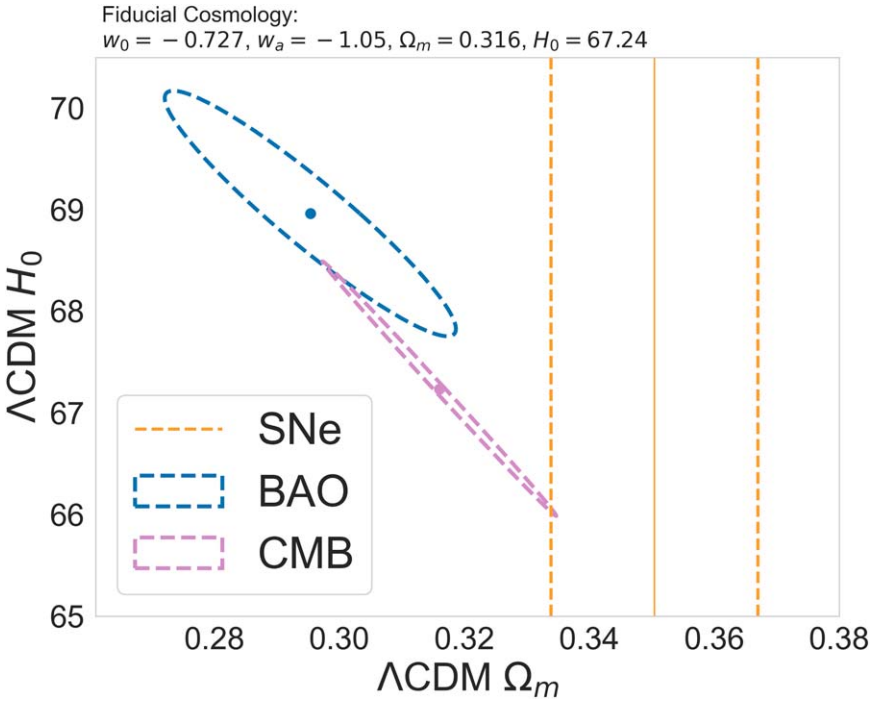

Figure 8. Fisher matrix constraints on Ω_m and H_0 under a ΛCDM framework derived from mock data sets under the best-fit w_0w_aCDM cosmology from DESI+DES-SN+Planck. The SN constraints are shown as vertical dashed lines with a solid central line (yellow), BAO constraints are represented by blue ellipses, and CMB constraints are shown as pink ellipses. The solid point/line is the maximum likelihood point calculated from Fisher. The fiducial cosmology is $\{w_0 = -0.727, w_a = -1.05, \Omega_m = 0.316, H_0 = 67.24\}$.

$$\boldsymbol{\theta}_{\mathrm{ML}}^{(\mathrm{CMB})} = \boldsymbol{\theta}_{\mathrm{fid}} + \boldsymbol{F}_{\mathrm{CMB}}^{-1}\, \boldsymbol{J}_{\mathrm{CMB}}^{T}\, \boldsymbol{C}_{\mathrm{P18}}^{-1} \Delta_{\mathrm{CMB}}.$$

The uncertainties in the parameters are given by the square roots of the diagonal elements of the inverse Fisher matrix:

$$\sigma_{\Omega_m}^{\mathrm{CMB}} = \sqrt{(\boldsymbol{F}_{\mathrm{CMB}}^{-1})_{11}}, \quad \sigma_{H_0}^{\mathrm{CMB}} = \sqrt{(\boldsymbol{F}_{\mathrm{CMB}}^{-1})_{22}}.$$

We present the constraints on Ω_m and H_0 derived from the Fisher matrix analysis applied to mock CMB, BAO, and SN data sets generated under the best-fit w_0w_aCDM cosmology from DESI+DES-SN+Planck (DESI Collaboration 2025): $\{w_0 = -0.727, w_a = -1.05, \Omega_m = 0.316, H_0 = 67.24\}$. The results are shown in Figure 8, where we plot the 68% confidence regions for each probe individually and their respective maximum likelihood estimates.

Additionally, the numerical results of our Fisher matrix analysis are summarized below:

1. SN results:

$$\Omega_m^{\mathrm{ML}} = 0.350 \pm 0.017.$$

2. BAO results:

$$\Omega_m^{\mathrm{ML}} = 0.295 \pm 0.015, \quad H_0^{\mathrm{ML}} = 68.96 \pm 0.80.$$

3. CMB results:

$$\Omega_m^{\mathrm{ML}} = 0.314 \pm 0.012, \quad H_0^{\mathrm{ML}} = 67.40 \pm 0.83.$$

The constraints presented in Figure 8 can be compared with those in Figures 1 and 6. In Figure 6, the BAO constraints are recalculated under the assumption of direct calibration of r_d, which aligns with our Fisher matrix results. Specifically, in our Fisher matrix analysis, the BAO calculations treat r_d as a constant, making the constraints more elongated and less circular in the Ω_m–H_0 plane compared to Figure 1. Our Fisher matrix results align closely with the findings in Figure 6, where direct r_d calibration is applied.

Appendix E
Null Tests

To validate our analysis methods, we performed a null test wherein we generated mock data sets under a consistent ΛCDM cosmology and analyzed them using the w_0w_aCDM cosmological model. This test aims to confirm that our pipeline correctly recovers the input cosmological parameters when there are no discrepancies among the probes and that it does not falsely indicate a preference for evolving dark energy.

We simulated SN, BAO, and CMB data sets using the same ΛCDM cosmology with $H_0 = 70$ km s^{-1} Mpc^{-1} and $\Omega_m = 0.30$. This choice ensures that all probes are consistent with each other and with the cosmological model used in the analysis.

We then performed the MCMC analysis on the combined mock data sets as in Section 3.1 and Appendix A, fitting them under the w_0w_aCDM model with additional free parameters. The likelihood function used is the same as in Section 2.

The best-fit parameters and their 68% confidence intervals for the combined data sets are as follows (H_0 in km s^{-1} Mpc^{-1} units):

Top panels of Figure 9: Gaussian prior on $\Omega_b h^2$:

$$\begin{aligned} \text{SNe + BAO:} \quad & \Omega_m = 0.30^{+0.03}_{-0.04} \quad w_0 = -0.99^{+0.07}_{-0.07} \\ & w_a = -0.05^{+0.64}_{-0.71} \quad H_0 = 70.21^{+2.46}_{-3.89} \\ \text{SNe + BAO + CMB:} \quad & \Omega_m = 0.30^{+0.01}_{-0.01} \quad w_0 = -0.99^{+0.06}_{-0.05} \\ & w_a = -0.03^{+0.25}_{-0.28} \quad H_0 = 70.02^{+0.59}_{-0.56}. \end{aligned}$$

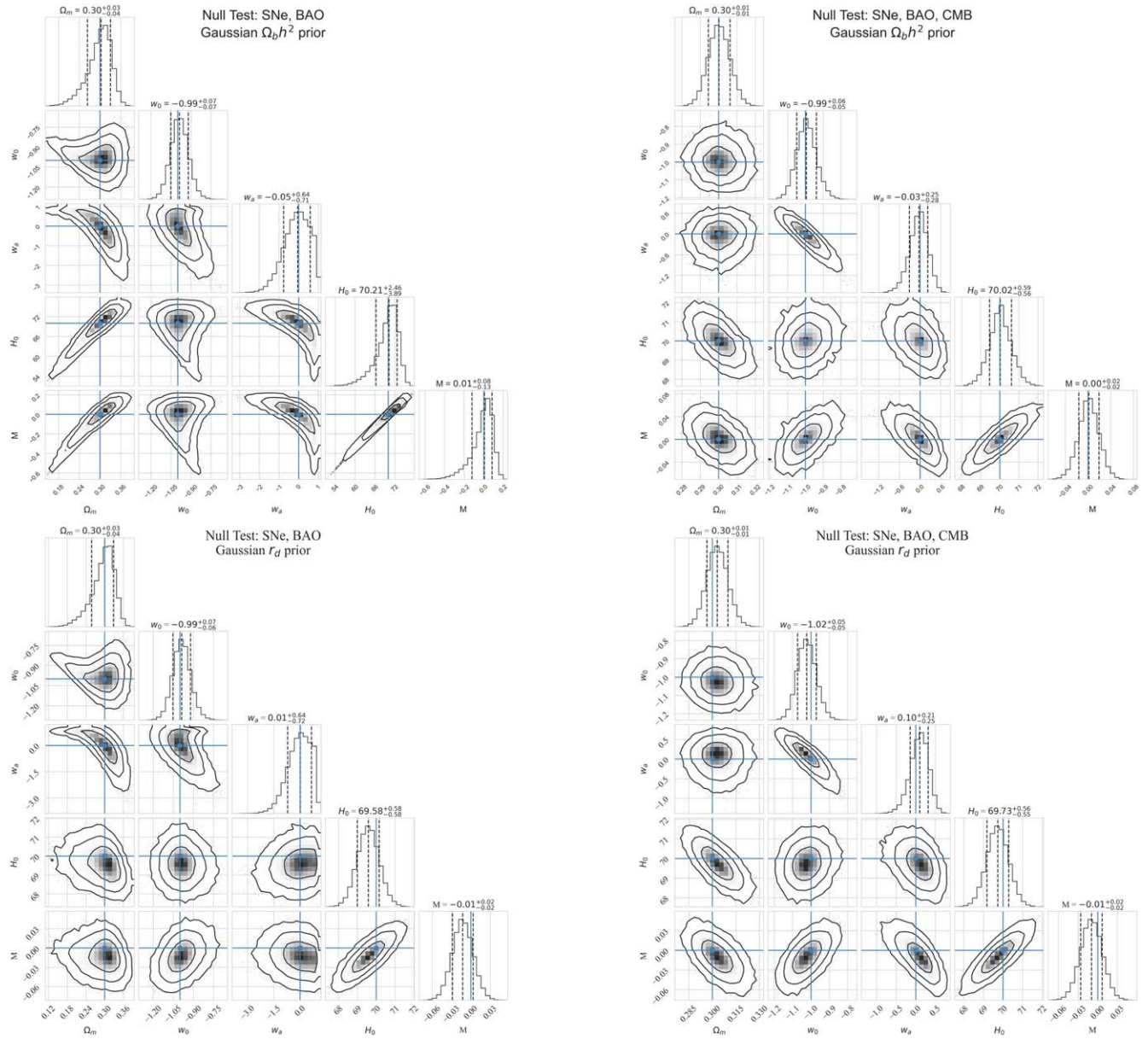

Figure 9. Null test: posterior distributions of Ω_m, w_0, w_a, and H_0 from the MCMC analysis of the combined data sets when the input is simulated under the same ΛCDM cosmology. The top two panels (left: SNe, BAO; right: SNe, BAO, CMB) adopt r_d derived using Equation (2.5) from the DESI Y1 paper, which has standard early-time physics assumptions, taking a Gaussian prior on $\Omega_b h^2 = 0.02218 \pm 0.00055$, the same as in Equation (2.9) in DESI Collaboration (2025). The bottom two panels (left: SNe, BAO; right: SNe, BAO, CMB) use a Gaussian prior on the sound horizon $r_d = 147.09 \pm 0.26$ Mpc. The input values $\Omega_m = 0.30$ and $H_0 = 70$ km s^{-1} Mpc^{-1} are indicated by blue lines, and the contours represent the 68%, 95%, and 99.7% confidence levels. All posteriors recover the input cosmology within 1σ.

Bottom panels of Figure 9: Gaussian prior on r_d:

$$\begin{aligned}
\text{SNe + BAO:} \quad & \Omega_m = 0.30^{+0.03}_{-0.04} \quad w_0 = -0.99^{+0.07}_{-0.07} \\
& w_a = 0.01^{+0.64}_{-0.72} \quad H_0 = 69.58^{+0.58}_{-0.58} \\
\text{SNe + BAO + CMB:} \quad & \Omega_m = 0.30^{+0.01}_{-0.01} \quad w_0 = -1.02^{+0.05}_{-0.05} \\
& w_a = 0.10^{+0.25}_{-0.21} \quad H_0 = 69.73^{+0.56}_{-0.55}.
\end{aligned}$$

The results of the MCMC analysis are shown in Figure 9, which displays the posterior distributions of Ω_m, w_0, w_a, and H_0. The blue lines indicate the input cosmological parameters used to generate the mock data ($\Omega_m = 0.30$, $w_0 = -1$, $w_a = 0$, $H_0 = 70$ km s^{-1} Mpc^{-1}). They all recover the ΛCDM results well.

Appendix F
Profile Likelihood Tests

While the main body of this Letter focuses on Bayesian and Fisher/Hessian-based approaches, here we present additional *profile likelihood* tests to validate the robustness of our conclusions to prior-volume effects. Profile likelihoods provide a complementary frequentist framework with a different treatment of nuisance parameters than standard Bayesian marginalization. They can be particularly illuminating if one suspects prior-volume effects or non-Gaussian shapes in the likelihood (L. Herold et al. 2024).

We construct the profile likelihood for each cosmological parameter using Procoli (T. Karwal et al. 2024) by fixing that parameter of interest to a grid of values while maximizing

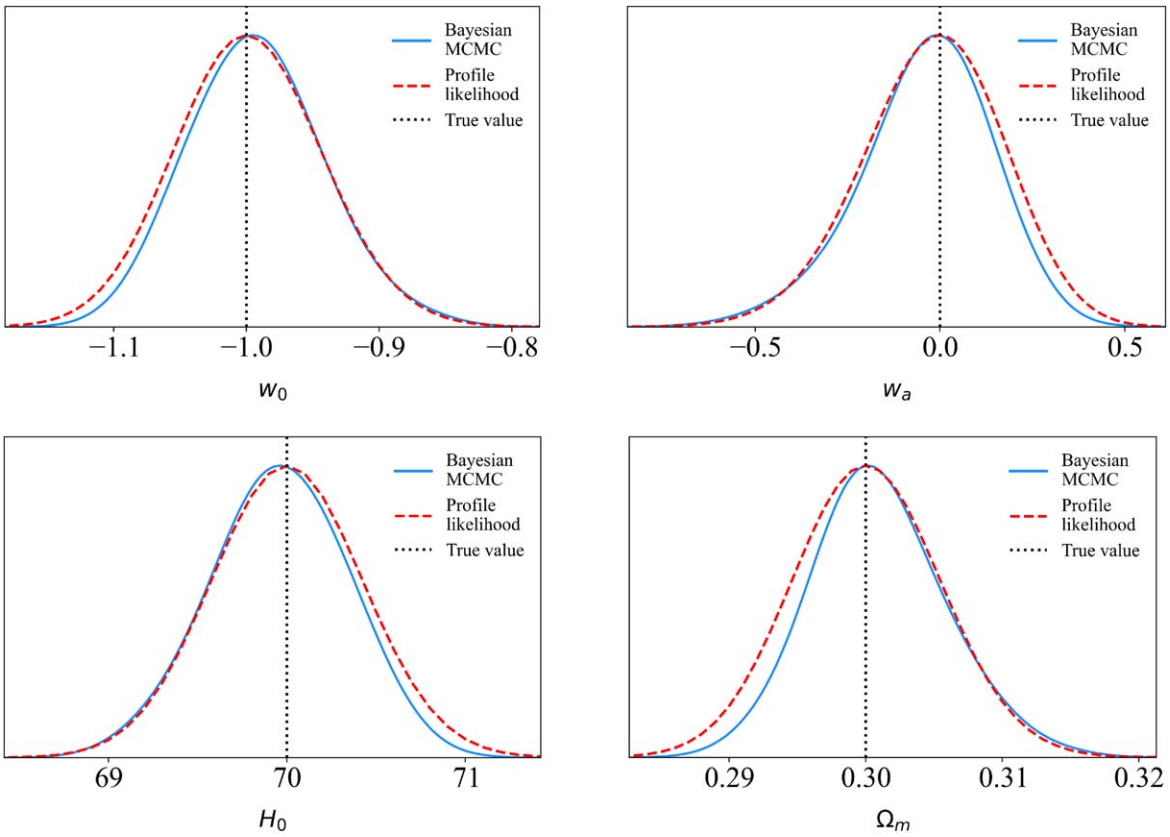

Figure 10. Illustrative profile likelihood curves (dashed) for cosmological parameters under the w_0w_aCDM model, compared with the 1D posterior from our MCMC fit (solid). These were generated for mock CMB, BAO, and SN data in a ΛCDM universe, marked by the dotted vertical lines.

(profiling) over all remaining parameters in the likelihood. We then compare these profile likelihood curves to our MCMC posteriors for the same simulated data sets (described in Section 2).

Figure 10 shows profile likelihood curves for w_0, w_a, Ω_m, and H_0 for the w_0w_aCDM cosmology. We find that the best-fit points and widths of the 1D profile likelihood constraints closely match the posteriors from our MCMC runs, showing the consistency of our fits.

Overall, the profile likelihood analysis confirms that for a universe that is truly ΛCDM and consistent across SN, BAO, and CMB data sets, jointly analyzing it under a w_0w_a cosmology does not introduce any biases in the posteriors of w_0, w_a, Ω_m, and H_0 due to prior-volume effects.

ORCID iDs

Xianzhe TZ Tang https://orcid.org/0009-0007-3185-7030
Dillon Brout https://orcid.org/0000-0001-5201-8374
Tanvi Karwal https://orcid.org/0000-0002-1384-9949
Chihway Chang https://orcid.org/0000-0002-7887-0896
Vivian Miranda https://orcid.org/0000-0003-4776-0333
Maria Vincenzi https://orcid.org/0000-0001-8788-1688

References

Armstrong, P., Qu, H., Brout, D., et al. 2023, PASA, 40, e038
Berghaus, K. V., Kable, J. A., & Miranda, V. 2024, PhRvD, 110, 103524
Brout, D., & Scolnic, D. 2021, ApJ, 909, 26
Brout, D., Scolnic, D., Popovic, B., et al. 2022a, ApJ, 938, 110
Brout, D., Taylor, G., Scolnic, D., et al. 2022b, ApJ, 938, 111
Brownsberger, S. R., Stubbs, C. W., & Scolnic, D. M. 2019, ApJ, 875, 34
Camilleri, R., Davis, T., Hinton, S., et al. 2025, MNRAS, 537, 1818
Cardelli, J. A., Clayton, G. C., & Mathis, J. S. 1989, ApJ, 345, 245
Chen, L., Huang, Q.-G., & Wang, K. 2019, JCAP, 2019, 028
DESI Collaboration 2024, ApJL, 973, L14
DESI Collaboration 2025, JCAP, 2025, 021
Dhawan, S., Brout, D., Scolnic, D., et al. 2020, ApJ, 894, 54
Fitzpatrick, E. L. 1999, PASP, 111, 63
Foreman-Mackey, D., et al. 2016, JOSS, 1, 24
Foreman-Mackey, D., Hogg, D. W., Lang, D., & Goodman, J. 2013, PASP, 125, 306
Harris, C. R., Millman, K. J., Van Der Walt, S. J., et al. 2020, Natur, 585, 357
Herold, L., Ferreira, E. G., & Heinrich, L. 2024, arXiv:2408.07700
Hinton, S. R. 2016, JOSS, 1, 00045
Karwal, T., Patel, Y., Bartlett, A., et al. 2024, arXiv:2401.14225
Kenworthy, W. D., Jones, D. O., Dai, M., et al. 2021, ApJ, 923, 265
Komatsu, E., Dunkley, J., Nolta, M., et al. 2009, ApJS, 180, 330
Mossa, V., Stöckel, K., Cavanna, F., et al. 2020, Natur, 587, 210
Planck Collaboration 2020, A&A, 641, A6
Popovic, B., Brout, D., Kessler, R., & Scolnic, D. 2023, ApJ, 945, 84
Rebouças, J., de Souza, D. H. F., Zhong, K., Miranda, V., & Rosenfeld, R. 2025, JCAP, 2025, 024
Riess, A. G., Yuan, W., Macri, L. M., et al. 2022, ApJL, 934, L7
Robitaille, T. P., Tollerud, E. J., Greenfield, P., et al. 2013, A&A, 558, A33
Rubin, D., Aldering, G., Barbary, K., et al. 2015, ApJ, 813, 137
Rubin, D., Aldering, G., Betoule, M., et al. 2023, arXiv:2311.12098
Rykoff, E. S., Tucker, D. L., Burke, D. L., et al. 2023, arXiv:2305.01695
Sánchez, B. O., Brout, D., Vincenzi, M., et al. 2024, ApJ, 975, 5
Scolnic, D., Brout, D., & Carr, A. 2022, ApJ, 938, 113
Tada, Y., & Terada, T. 2024, PhRvD, 109, L121305
Taylor, G., Lidman, C., Tucker, B. E., et al. 2021, MNRAS, 504, 4111
Vincenzi, M., Brout, D., Armstrong, P., et al. 2024, ApJ, 975, 86
Virtanen, P., Gommers, R., Oliphant, T. E., et al. 2020, NatMe, 17, 261